Patterns and drivers of population trends on individual Breeding Bird Survey routes using spatially explicit models and route-level covariates.

Adam C. Smith, Veronica Aponte, Allison D. Binley, Amelia R. Cox, Lindsay Daly, Courtney Donkersteeg, Brandon P.M. Edwards, Willow B. English, Marie-Anne R. Hudson, David Iles, Kendall Jefferys, Barry Robinson, Christian Roy

Adam C. Smith – adam.smith@ec.gc.ca, Canadian Wildlife Service, Environment and Climate Change Canada, Ottawa, ORCID: 0000-0002-2829-4843

Veronica Aponte - Canadian Wildlife Service, Environment and Climate Change Canada, Ottawa,

Allison D. Binley - Department of Biology, Carleton University, Ottawa, Canada ORCID: 0000-0001-8790-9935

Amelia R. Cox - Canadian Wildlife Service, Environment and Climate Change Canada, Yellowknife, Canada

Lindsay Daly - Canadian Wildlife Service, Environment and Climate Change Canada, Ottawa, ORCID: 0000-0002-0892-5505

Courtney Donkersteeg - Department of Biology, Carleton University, Ottawa, Canada

Brandon P.M. Edwards, Department of Biology, Carleton University, Ottawa, Canada & Canadian Wildlife Service, Environment and Climate Change Canada, Ottawa, ORCID: 0000-0003-0865-3076

Willow B English - Canadian Wildlife Service, Environment and Climate Change Canada, Ottawa, ORCID: 0000-0002-0863-8581

Marie-Anne R. Hudson - Canadian Wildlife Service, Environment and Climate Change Canada, Ottawa, ORCID: 0000-0002-9599-0697

Kendall M Jefferys - Environmental Change Institute, School of Geography and the Environment, University of Oxford, Oxford, UK ORCID: 0000-0003-4439-9394

Barry Robinson - Canadian Wildlife Service, Environment and Climate Change Canada, Edmonton Canada ORCID: 0000-0002-2646-2508

Christian Roy - Canadian Wildlife Service, Environment and Climate Change Canada, Gatineau, Canada ORCID: 0000-0002-5599-6234

Acknowledgements:

We sincerely thank the thousands of U.S. and Canadian participants and the regional and national coordinators who have conducted and coordinated the North American Breeding Bird Survey for almost 60 years.

Author Contributions:

All authors contributed to the conceptual development of the ideas and concepts, study design, editing and drafting of the text. ACS, ARC, KMJ, and CR conducted the analyses.

Data Availability

Analyses reported in this article can be reproduced using the data and code provided at https://github.com/AdamCSmithCWS/Route-level_BBS_trends. (this will be permanently archived on publication)

Keywords

Ecological Monitoring, Gaussian Process, iCAR, population abundance

Abstract

Spatial patterns in population trends, particularly those at fine geographic scales, can help better understand the factors driving population change in North American birds. The standard trend models for the North American Breeding Bird Survey (BBS) were designed to estimate changes in relative abundance through time (trend) within broad geographic strata, such as countries, Bird Conservation Regions, U.S. states, and Canadian territories or provinces. Calculating trend estimates at the level of the BBS's individual survey transects ("routes") allows exploration of finer spatial patterns and estimation of the effects of covariates, such as habitat loss or annual weather, on both relative abundance and trend. Here, we describe four related hierarchical Bayesian models that estimate trends for individual BBS

routes. All four models estimate route-level trends and relative abundances using a hierarchical structure that shares information among routes, and three of the models share information in a spatially explicit way. The spatial models use either an intrinsic Conditional Autoregressive (iCAR) structure or a distance-based Gaussian Process (GP) to estimate the spatial components. We fit all four models to data for 71 species and then, because of the intensive computations required, fit two of the models (one spatial and one non-spatial) for an additional 216 species. In a leave-future-out cross-validation, the spatial models outperformed the non-spatial models for 284 out of 287 species. The best approach to modeling the spatial components depends on the species being modeled; the Gaussian Process had the highest predictive accuracy for 69% of the species tested here and the iCAR was better for the remaining 31%. We also present two examples of route-level covariate analyses focused on spatial and temporal variation in habitat for Rufous Hummingbird (*Selasphorus rufus*) and Horned Grebe (*Podiceps auritus*). In both examples, the inclusion of covariates improved our understanding of the patterns in the rate of population change for both species. Route-level models for BBS data are useful for visualizing spatial patterns of population change, generating hypotheses on the causes of change, comparing patterns of change among regions and species, and testing hypotheses on causes of change with relevant covariates.

Introduction

The North American Breeding Bird Survey (BBS) is a major source of information on the changes in North American bird populations at broad spatial scales. Since 1966, the BBS has provided trend information at broad geographic scales (range-wide, national, and regional) across much of Canada and the United States for up to 500 species of birds (Hudson et al. 2017, Sauer et al. 2017). BBS data are collected annually by expert volunteers conducting 50, 3-minute point-counts along a roughly 40-km long roadside route, and approximately 5000 routes are surveyed each year (Hudson et al. 2017). The field methods are designed to estimate changes in relative abundance through time by controlling for the effects of survey location, weather, time of day, and season, as well as variations among observers (Sauer et al. 2003).While the BBS is an excellent source of information on trends, its road-side surveys may not capture all species. Similarly, although the roadside locations are generally representative of the surrounding landscape in most regions (Veech et al. 2017), in some regions it may not represent changes in the landscape far from roads (Van Wilgenburg et al. 2015). It also does not include the information needed to directly model variations in detectability, instead relying on the strictly controlled field methods and statistical adjustments for the most likely sources of variation. These potential sources of bias in BBS trends have been studied and reviewed (e.g., Sauer et al. 2017), and with some care in interpreting the results, BBS trend estimates provide important conservation information (Rosenberg et al. 2017). The BBS was designed to monitor changes in species' populations over time across broad regions such as the intersection of states/provinces with Bird Conservation Regions (Sauer et al. 2003, Link et al. 2020, Smith and Edwards 2021). BCRs are regions of North America, similar to ecoregions (CEC 1997) that share similar ecological characteristics as well as similar bird communities (Bird Studies Canada and North American Bird Conservation Initiative 2014). These regional-scale summaries are critical for identifying and prioritizing species in peril (Government of Canada 2010, IUCN 2012, Rosenberg et al. 2017) and understanding broad-scale patterns of change in North American birds (North American Bird Conservation Initiative Canada 2019, Rosenberg et al. 2019, North American Bird Conservation Initiative 2022).

The BBS dataset can also be analyzed at a finer spatial resolution to complement the regional estimates, and to inform different ecological questions and conservation efforts. Fine-scale estimates of trends should benefit from including the spatial relationships among individual survey locations (e.g., Smith et al. 2024), and allow for visualizing spatial patterns in trends to better understand the local context of range-wide trends and to generate hypotheses on the drivers of population trends. Compared to regional estimates, fine-scale estimates of population trends may provide more useful information for local conservation efforts, as covariates with local effects such as local land cover change, and agricultural practices can be modeled (Thogmartin et al. 2004, Paton et al. 2019, Mirochnitchenko et al. 2021). Many factors influence the relative abundance and trends in bird populations, and they act and interact to induce spatial patterns across a range of spatial scales (Morrison et al. 2010). Factors such as habitat change (Stanton et al. 2018, Betts et al. 2022), biotic factors like prey availability (Drever et al. 2018), or broad-scale patterns in abiotic factors like precipitation, temperature, and phenology (Renfrew et al. 2013, Wilson et al. 2018) can induce spatial patterns in trends or relative abundance and can act across different periods in the species' annual cycles (Morrison et al. 2010, Wilson et al. 2011). Likewise, conservation actions occur at many scales, from the broad scales of international conventions to the fine scales of an individual wetland (Prairie Habitat Joint Venture 2020).

Including both relative abundance and trend as parameters can improve our understanding of population change, by separately modeling the pattern and covariates that affect the variation in relative abundance in space (e.g., distribution, range dynamics, habitat availability) from those that affect changes in abundance through time (e.g., habitat change, weather and climate). Earlier fine-scale models for the BBS data did not include the rate of population change (trend) as a parameter in the model (Bled et al. 2013). However, including both relative abundance and trends as separate parameters allows the model to include covariates on each, such as a recent analysis of the effects of forest change on species' trends on BBS routes (Betts et al. 2022). A spatially-explicit hierarchical regression can model both spatial patterns in relative abundance and trend (Ver Hoef et al. 2018, Wright et al. 2021). Here we use the term

121 "hierarchical" model in a general sense to describe models with layered structures where parameters at
122 one level are drawn from distributions and the parameters of those distributions are modeled at higher
123 levels (Cressie et al. 2009, Gelman et al. 2013, Kruschke 2015). Separating these parameters in the model
124 allows for the inclusion of a broader range of covariates (Meehan et al. 2019) to better understand the
125 processes affecting relative abundance (e.g., mean habitat amount or distance to core of a species' range)
126 and trends (habitat change through time, or differences in climate change effects at Northern or Southern
127 range limits).

128 One goal of our work here is to compare two conceptually different approaches to modeling spatial
129 relationships because the spatial locations of BBS observations are not perfectly represented by either of
130 the most common approaches. Spatially explicit models treat sample locations as either discrete areas
131 with neighborhood relationships (Ver Hoef et al. 2018), or points within continuous space (Golding and
132 Purse 2016). It is not obvious whether an area-based or point-based approach better reflects reality for
133 BBS data (Pebesma and Bivand 2023), because the observations from a given BBS route are collected
134 along a transect that is approximately 40 km long. Intrinsic Conditional Autoregressive (iCAR) structures
135 are area-based and model space as a network of polygons with binary neighborhood relationships, e.g.,
136 only polygons sharing a border are considered neighbours (Besag and Kooperberg 1995). This area-
137 based approach has been used to model the relatively fine-scale population trends in Christmas Bird
138 Count data (Meehan et al. 2019) and the annual relative abundance of birds using BBS data (Bled et al.
139 2013). Gaussian Process (GP) models use a continuous measure of distance between points to estimate
140 the correlation of parameters (e.g., trends) between pairs of points and the rate of decrease in the
141 correlation with increasing distance (Golding and Purse 2016). Both approaches are necessary
142 simplifications of the true spatial processes underlying variation in relative abundance and trends among
143 BBS routes. The iCAR approach simplifies the spatial structure by assuming each route represents a
144 discrete area of space (i.e. a polygon surrounding the route; Figure 1), but the neighboring routes may be
145 separated by a wide range of distances depending on the spatial distribution and spatial density of those

routes. The GP approach simplifies spatial relationships by assuming each route represents a point in space, but the measure of intervening distance among routes only applies to the distance between the start points, not to the full transect.

Here we describe and compare four fine-scale BBS models that expand on the published broad-scale BBS models in three ways: 1) they estimate bird population trends and relative abundance at a fine-scale (individual BBS routes); 2) they allow for route-level covariates on the trends and relative abundances; and 3) their output visualizes spatial patterns in both trend and relative abundance. Most of the models share information on relative abundance and trend in a spatially explicit way, and we have included a non-spatial model for comparison. We describe two spatial models that rely on an iCAR structure for the spatial relationships: the first is the iCAR model; and the second is a version of the BYM model, named for Besag, York, and Mollié (Besag et al. 1991), which is identical to the iCAR model but includes an additional random effect to allow extra non-spatial variation in trends. The third spatial model is an isotropic Gaussian Process (GP) model that models spatial relationships using the Euclidean distances among routes. Finally, the fourth model is a non-spatial version that estimates route-level variation in trends and relative abundances as a log-normally distributed random effect. We fit all four models to 71 species and fit one of the spatial models (iCAR) and the non-spatial model to an additional 216 species (details below). We compare the predictive accuracy of models in a leave-future-out cross-validation to assess the benefits of including spatial information and to compare the various approaches to modeling space for the BBS data. Finally, we provide two examples of route-level covariate analyses, to demonstrate the application of these models to conservation and research into understanding the drivers of population change and how those drivers may vary in space and time.

Methods

Data

We limited most of our analyses to a 15-year period, which we considered short enough that the log-linear slope that represents population trends in these models can be a meaningful summary of the population change (Buckland et al. 2004, Thompson and La Sorte 2008). In effect, 15 years is likely long enough to estimate a rate of change on each route, but also short enough to reduce the likelihood of complex non-linear population patterns. The only exception is the Horned Grebe covariate example, where we used a 43-year period because the covariate was designed to adjust for annual fluctuations and non-linear patterns in regional moisture/drought cycles (details below). This 15-year period is somewhat arbitrary and for many species or ecological questions, it may be very informative to fit these models (or modifications of these models) to longer or shorter periods of time.

We used 71 species (Table S1) to compare the model predictions and predictive accuracy for all four models and used the Baird's Sparrow (*Centronyx bairdii*) to demonstrate model fit and convergence. We chose these 71 species because they have small ranges with relatively few BBS routes, which improves computational efficiency, and yet are also commonly observed during surveys and so provide high-quality data on any given route. We chose the Baird's Sparrow to demonstrate model fit and convergence, as it has some interesting spatial variation in abundance and trends and a very restricted distribution confined to the northern Great Plains region (Figure 1), which reduces model run-time. Species with large ranges that appear on many routes will increase the computational power required to run the models, increasing the model run-time. Specifically, from 2006 to 2021, these small-range species were observed on 125-400 BBS routes, with at least 600 total observations of the species and an average of at least four observations per route. These thresholds on numbers of routes and observations are effectively arbitrary, but balanced the need to have sufficient count-data to estimate parameters well and few enough routes that models would fit relatively quickly. We only compared the fit and predictive accuracy of all four models for these

species with fewer than 400 routes, because fitting the GP model requires days or even weeks for species with many routes.

To better understand the benefits of including space in a model for more species, we compared the non-spatial model and one of the spatial models for an additional 216 species that have larger ranges. For these species, we only compared the predictions and predictive accuracy of the non-spatial model to the iCAR model, to reduce our computations. These 216 species were observed on 400 or more BBS routes during 2006-2021 (i.e., species with more routes than the small-range species). We fit these two models to these additional species to assess the more general benefits of including spatial information for more species and for species with populations spread across large ranges that may include many different factors influencing trends and relative abundance (Doser et al. 2024).

Model structure

The four models are hierarchical log-link negative binomial regressions broadly similar to other models commonly applied to BBS data (Sauer and Link 2011, Smith et al. 2014), but modeling trend and relative abundance as route-specific, spatially varying coefficients (Barnett et al. 2021, Thorson et al. 2023, Doser et al. 2024). In all four models, each route has a separate slope (trend) and intercept (relative abundance), but there are no parameters to model yearly fluctuations or non-linear temporal patterns. Therefore, the interpretation of "trend" in these models is limited to this log-linear slope parameter (i.e., a single mean rate of change over the entire modeled time-series).

All of the models have the same basic structure (Figure 2), varying only in the way the intercept and slope terms were estimated (Figure 3). In all models, we treated BBS counts as being drawn from a negative binomial distribution (equation 1 and 2, Figure 2). We included the same observer effects commonly included in BBS trend models (Smith et al. 2024), keeping the observer effects (equation 5, Figure 2), the inverse dispersion parameter (equation 3, Figure 2) and the first-year observer effects (equation 4, Figure 2) in all models. We included the first-year BBS observer parameter, as first-year observers have distinct variations in their counts of some species when compared to more experienced observers (Kendall 1996).

Route-level intercepts (alpha terms highlighted in lighter yellow, Figure 3) and route-level slope parameters (beta terms highlighted in darker green, Figure 3) were estimated as hierarchical effects, sharing information among routes. Specifically, both the intercepts and the slopes were estimated as an additive combination of a species-mean and a random route-level term (equations 4 and 5, Figure 3). Three of the models used spatial information to estimate the route-level variation in the intercepts and slopes (i.e., effectively shrinking towards a local mean of neighboring routes), while the fourth non-spatial model estimated them as exchangeable random effects (i.e., shrinking towards a global mean of all routes). To encourage convergence, we constrained many of the random effects in the model, including the spatial route-level parameters, to sum to zero. These constraints often improved model sampling efficiency, but because they are centered on a mean across all routes, they do not affect the interpretation of the final route-level slopes or intercepts (Morris et al. 2019).

To estimate route-level relative abundance, while accounting for variation among observers, we modeled separate intercepts for routes and observers. Using separate observer and route effects has not been commonly included in hierarchical Bayesian models for the BBS (Sauer and Link 2011, Smith et al. 2014, Link et al. 2020, Edwards and Smith 2021), until recently (Betts et al., 2022, Smith et al., 2024). In general, observers and routes are partly associated in the BBS dataset by design as an experimental control for variation among observers (Kendall et al. 1996). However, observers and routes vary in the number of surveys conducted, from 2006-2021 more than 69% of surveys were conducted on routes with more than one observer during those 15 years, and 55% of surveys were conducted by observers who have surveyed more than one route.

Finally, we also used an informative prior on the standard deviation of the observer effects (equation 6, Figure 2), and we ensured that all parameters had converged when fitting the models (details below). We used a half-normal prior on the standard deviation among observers, scaled so that variation among observers is unlikely to result in a six-fold increase, or reduction, in a given species count (equation 6, Figure 2), and that variation among observers is less than variation among routes. We suggest this prior is

reasonable given that BBS observers are highly skilled and familiar with the local bird community (Link and Sauer 1997).

Spatial structures

We fit models with two different approaches to account for spatially explicit relationships among routes: 1) an intrinsic Conditional Autoregressive (iCAR) structure that treats spatial relationships as a series of discrete neighbors, producing a sparse matrix of adjacencies between pairs of routes; and 2) an isotropic Gaussian process (GP) model that treats space as the continuous distance between routes, creating a matrix of Euclidean distances between the start locations of each BBS route. To illustrate one difference between the approaches, the GP may consider the relative abundance or trends of two distant routes as effectively independent if the distance is large enough. In contrast, the iCAR structure considers any routes whose polygons share a border as having a very close connection, regardless of polygon size or distance. In some cases, treating two relatively distant routes as close neighbors may be useful if their relative proximity could inform the parameter estimates, but may also introduce error into the estimate of spatial variance (Pebesma and Bivand 2023).

We used a Voronoi tessellation to generate the discrete neighborhood relationships required to support the iCAR model (Ver Hoef et al. 2018, Pebesma and Bivand 2023). iCAR models are often applied to contiguous area-based stratifications, such as regular grids, census regions, or political jurisdictions, which have natural neighborhood relationships defined by their adjacencies (Ver Hoef et al. 2018, Meehan et al. 2019). To generate contiguous discrete spatial units without imposing a regular grid structure, we used a Voronoi tessellation to create contiguous polygons, centered on the start point of each BBS route (Pebesma 2018). We further limited the adjacency matrix to the approximate boundaries of the species' range by clipping the tessellated surface using the BBS strata where the species occurs (Sauer and Link 2011) and a concave polygon surrounding start locations of all routes with data for that species (Gombin 2023). This clipping ensured that adjacency relationships did not extend beyond the borders of

the species' range and allowed the adjacency matrix to respect large-scale, complex range boundaries (e.g., gaps in forest bird ranges created by the great plains).

We adapted functions and code in the Stan probabilistic programming language from the "rethinking" R-package for inclusion in our GP model (McElreath 2023). Like the iCAR approach, we used independent GPs to model the covariance of the intercept parameters and the slope parameters. We estimated the full matrix for between-route distances using functions in the "sf" package for R (Pebesma 2018).

Intrinsic Conditional Autoregressive model - iCAR

We estimated the route-level intercepts and slopes using an iCAR structure, where the parameter for route-r is drawn from a normal distribution, centered on the mean of that parameter's values in all neighboring routes, with an estimated standard deviation that is proportional to the inverse of the number of neighbors for that route (Morris et al. 2019). Specifically, the route-level variation in the intercept term a random route-level term drawn from a normal distribution centered on the mean of the intercepts for all neighboring routes (equation 6, Figure 3). The route-level variation in the slope was estimated similarly as a random draw from a normal distribution centered on the mean of the slopes for all neighbouring routes (equation 7, Figure 3).

Besag York Mollié iCAR model - BYM

We also used an implementation of the Besag, York, Mollié (BYM) spatial iCAR model (Besag et al. 1991) to estimate route-level slopes. The route intercepts were estimated in the same way as for the iCAR model (equation 6, Figure 3). The route-level variation in slopes used the same structure as for the iCAR model (equations 8 and 9, Figure 3), but we added a non-spatial component, estimated as a random effect drawn from a normal distribution with an estimated standard deviation (equation 10, Figure 3).The additional random effect in the BYM model allows the route-level trend estimates to vary more among neighboring routes, if supported by the data (Besag et al. 1991).

Gaussian Process model - GP

In the Gaussian Process (GP) model, the route-level variation in slope and intercept random terms were estimated as multivariate normal distributions (equations 11 and 12, Figure 3), with covariance matrices estimated using a squared exponential kernel function (Gelman et al. 2013, pg 501). The covariance terms for the intercept and slope parameters were separately estimated and are each an exponentially decreasing function of the distance between the routes (equations 13 and 14, Figure 3).

Non-spatial model

To assess the benefits of the spatially-explicit models, we compared the predictions and predictive accuracy of the spatial models to an otherwise identical model that lacked spatial information. This non-spatial model had all the same parameters as the spatial models, except that the route-level variation in the intercepts and slopes were estimated as random effects (equations 15 and 16, Figure 3).

Convergence

We fit all models using 1000-2000 warmup iterations and an equal number of sampling iterations for each of the four independent chains (or three independent chains for each iteration of cross-validation). We assessed convergence by monitoring for divergent transitions and estimating split-Rhat values and bulk effective sample sizes for all parameters. We considered convergence to have failed if any Rhat was > 1.03 or if any parameter's effective sample size is < 100 (although the vast majority of parameters had effective sample sizes > 1000 and Rhat < 1.01). For a few GP models that failed to converge, we re-fit the models with the alternative priors described in the supplemental methods.

Model assessment

To assess the benefits of adding spatial information into the model, we compared the 1-year-ahead, leave-future-out (LFO) predictive success of the four models for the 71 species with relatively small ranges (Roberts et al. 2017, Bürkner et al. 2020). In this application of LFO, we fit the model to the first eight years of data (2006-2013; the minimum length of time we considered sufficient for prediction), and used

313 the parameter estimates from this model to predict the counts in the following year (2014). Then we
314 iterated this approach making predictions for the remaining years (2015-2019, and 2021), predicting the
315 held-out data in year using data for all years prior to fit the model. We could not assess predictive
316 accuracy for the year 2020 because the BBS survey season was canceled due to the public health travel
317 restrictions of spring 2020. We also compared the iCAR spatial model with the non-spatial version of the
318 model using a LFO assessment for an additional 216 species (Table 1). We used the LFO approach to
319 directly test the accuracy of predictions for the next year's observations.

320 The cross-validation process generated predictions for every count in the dataset after 2013 and an
321 estimate of the log pointwise predictive density (lppd) of the observed count, given the model and the data
322 in all previous years (Gelman et al. 2014). The lppd is a metric of predictive accuracy that measures how
323 likely it would be to observe the held-out data point (i.e., the observed count in the next year) given the
324 parameter estimates and the model. More specifically, it is the log of the posterior probability (or
325 probability density) of each held-out data point (pointwise), given the model and parameter estimates.
326 Values of lppd are negative (log of probability values, which are < 1.0), and values closer to 0 indicate
327 predictions that are similar to the observed data. For interpretation and visualization, we calculated
328 pairwise differences in lppd between pairs of models for each count and transformed summaries of these
329 lppd differences across all counts into approximate z-scores (mean divided by the standard error of the
330 point-wise differences in lppd). These z-scores summarise the support in the data for each model,
331 accounting for the variation across all observations and providing a consistent scale to summarize pair-
332 wise model comparisons across datasets with different numbers of observations (Link and Sauer 2016).
333 They are an approximation of the test statistic in a paired t-test; e.g., absolute values greater than
334 approximately 2 could be interpreted as a "significant difference" in predictive success, although we have
335 avoided emphasizing arbitrary thresholds.

Route-level covariate examples

Modeling covariates of fine-scale trends and relative abundances is a major benefit of modeling BBS data at the route level. Including covariates, we can investigate conservation and management concerns such as estimating the effects of local habitat change on population trends, or the effects of moisture and climate on local abundance. Further, a fine-scale allows for the use of finer-scale, more localized covariates. To demonstrate this, we present two examples, each including route-level predictors to inform estimates of relative abundance and trend. The first example uses data on habitat suitability from an independent study (Jefferys et al. 2024) on the Rufous Hummingbird (*Selasphorus rufus*) and models the effect of habitat suitability on relative abundance and change in habitat suitability on trends in BBS data (see Jefferys et al. 2024 and supplemental methods). The second example looks at the effects of annual variation in available habitat—the number of ponds surrounding a BBS route each year in the Prairie Pothole Region (PPR)—on the expected counts of a water bird, the Horned Grebe (*Podiceps auratus*).

Rufous Hummingbird covariate example

This example model estimates the effect of the amount of suitable habitat around a BBS route on the mean number of birds observed, and the effect of the change in suitable habitat on the change in the number of birds observed through time. This example application is an elaboration of the iCAR route-level trend model, where the route-level intercepts and slopes are additive combinations of two components: 1) one that is a function of a route-level predictor, and 2) one that is a residual component, estimated as a spatially varying component using the iCAR structure (Ver Hoef et al. 2018). As with our previous models, this model used data from the BBS to estimate relative abundance and trend. The route-level predictors are derived from an independent study on Rufous Hummingbirds (Jefferys et al. 2024). In that study, habitat suitability was estimated with a species distribution model using an independent dataset of Rufous Hummingbird observations and data on weather, climate and landcover and changes in suitability were driven by the loss of early successional forest and warming temperatures in the northeastern regions of the breeding range (Jefferys et al. 2024). In our model, we used the mean habitat

suitability from that study across a 15-year period (2006-2021) in a 200m buffer surrounding each BBS route as a predictor on the intercept (i.e., mean habitat suitability as a predictor on the mean relative abundance on a given route). We used the rate of change in habitat suitability over the same 15-year period within the same buffer as a predictor on the slope (i.e., change in habitat suitability as a predictor on the trend).

We estimated the route-level variation in intercepts and slopes by extending equations 4 and 5 (Figure 3), to include a component that was a function of the mean habitat suitability for the intercept and the rate of change in habitat suitability for the slope (equations 17 and 18, Figure 4). The intercepts and slopes for each route were an additive combination of a mean species-level intercept or slope spatially varying residual component (equations 6 and 7, Figure 4), and a component that was a function of the mean habitat suitability on the route (equations 19 and 20, Figure 4) or rate of change in habitat suitability on the slope (equations 21 and 22, Figure 4).

This partitioning of the intercept and slope parameters allows the model to generate two alternative estimates of the mean relative abundance and trend on each route. The full trend (equation 18, Figure 4) represents the estimated trend on a given route, including the effects of habitat change. The residual trend (i.e., removing the final term from equation 18, Figure 4) represents an alternate trend if habitat suitability stayed constant on a given route. A similar partitioning of the residual and full estimates of the intercepts is possible, although we did not explore that here.

Horned Grebe covariate example

This example application was an elaboration of the iCAR route-level trend model, where trends and relative abundances are estimated while accounting for the annual variation in climatically dependent habitat. The route-level predictors are derived from a study of the effects of moisture/drought patterns on Horned Grebe (more detail in the supplemental methods), a waterbird species that breeds in small to moderately sized shallow, freshwater ponds (Stedman 2020). To represent annual variation in available

habitat for the Horned Grebe in the Canadian Prairie Pothole Region (PPR), we used a dataset collected collaboratively by the U.S. Fish and Wildlife Service (USFWS) and the Canadian Wildlife Service (CWS) across the entire PPR. From this dataset, we used only the Canadian data on the number of ponds (natural or artificial ponds that are flooded seasonally, semi-permanently, and permanently) during the Waterfowl Breeding Population and Habitat Survey (Smith 1995). Annual fluctuations in moisture affect the number of wetlands available, which in turn has a strong influence on waterbird populations that depend on wetlands (Sorenson et al. 1998, Johnson et al. 2005, Roy 2015, Steen et al. 2016). The model was based on the iCAR model and added an additional iCAR component to create a varying-coefficient model on the effects of available habitat on the expected counts during a given survey on a given route. We also fit the same species data to a simpler iCAR model with no covariates to compare the difference in estimated trends with and without accounting for the annual variations in available habitat.

Results

In general, there are clear spatial patterns in the estimated trends and relative abundances from the spatial models, with similar patterns among the three types of spatial models. Those patterns are obscured or completely lacking from the non-spatial version of the model (e.g., the results for Baird's Sparrow in Figures 5 and 6). The GP model tended to smooth the spatial pattern in trends more than the iCAR model, which in turn smoothed more than the BYM model (Figure 5). The spatial smoothing in relative abundance was stronger in both the iCAR and BYM models than the GP model for Baird's Sparrow (Figure 5). The covariance in relative abundance of Baird's Sparrow among routes was effectively 0 at distances of only 100 km, whereas the covariance in trend was relatively strong even at distances > 1000 km (Figure S1). Predictions of route-level trends had smaller standard errors when including spatial information, and trend precision generally increased with the degree of spatial smoothing (Figures 6, S2 and S3). For Baird's Sparrow, all three spatial models had better predictive accuracy than the non-spatial model, with z-scores of pairwise differences between one of the spatial models and the non-spatial model ranging from 2.7 – 3.3 (Figure S4). The iCAR model had better predictive accuracy than the BYM model

(z-score of the difference = 3.8; Figure 7), and there was little difference in predictive accuracy between the iCAR and GP models (z-score difference = -0.51; Figure 7).

The leave future out (LFO) cross-validation shows that the iCAR and GP models out-perform the non-spatial model (i.e. more accurately predicted the next year's data) for almost all the 71 small-range species (Figure 7 and Figure S4). Out of the spatial models, the GP model had the highest predictive accuracy for the greatest number of species, followed by the iCAR model and the BYM model had the lowest predictive accuracy. The BYM model was the only spatial model that had clearly lower predictive accuracy than the non-spatial model for any species (i.e., four species for which the z-score difference is < -2, Figure 7 and Figure S4). The iCAR model and the GP model had comparable predictive accuracy for many species (most values between -2 and +2 in the iCAR-GP comparison of Figure 7); 69% (49 of 71 species) of the species were better predicted by the GP model (negative values Figure 7) and the remaining species were better predicted by the iCAR model (positive values in Figure 7). When including the additional 216 species for which fitting the GP model was prohibitively time-consuming (days or even weeks are required for convergence for a given species), the iCAR spatial model had higher predictive accuracy than the non-spatial model for 283 of 287 species, and predictive accuracy was very similar for the remaining four (Figure 8).

The iCAR model generated trend prediction maps with clear spatial patterns that likely relate to spatially dependent variation in processes affecting populations (Figure 9). These patterns are not evident in predictions from an identical model without spatial information (Figure 9). The spatial patterns in route-level trends vary widely among these species and among the others we tested (Figures S2 and S3), suggesting varied drivers of population change across the continent and among species.

In general, the iCAR and GP models were comparable in predictive accuracy for the 71 small-range species we analyzed (Figure 7). In addition, the spatial patterns in predicted trends were very similar between these two models, even for species where the predictive accuracy differed between the models (Figure 10). For example, the GP model had higher predictive accuracy than the iCAR model (z-score

435 difference = -4.3, Figure S4) for Canyon Towhee (*Melozone fusca*), but the opposite was true for Western
436 Bluebird (*Sialia mexicana*; z-score difference = 2.3, Figure S4). Regardless, the spatial pattern in
437 predicted trends between the two models is quite similar for both species (Figure 10). For both species,
438 and in general, the GP model trend estimates had narrower credible intervals (higher estimated precision)
439 than the iCAR model (Figure S5 and S6). Precision of the iCAR trend estimates also showed a clear
440 relationship to the number of neighbors for any given route, in that routes with few neighbors (on the
441 edges of the species' range) were much less precise than estimates in the core of the species' range
442 (Figure S6).

443 Including habitat suitability in the Rufous Hummingbird population model affected estimates of route-
444 level relative abundance and improved estimates of the spatial pattern in trends (Figure 11). However,
445 much of the overall decline was not related to covariates describing route-level habitat change, as the
446 negative population trends across the species' range remained after removing the effects of local habitat
447 change covariates (right panel, Figure 11). The effect of habitat suitability on mean relative abundance
448 was strong and positive (ρ_α = 3 [95% CI 2.2:3.8]), such that routes with higher overall habitat suitability
449 had higher mean counts. From 2006-2021, the Rufous Hummingbird's overall population declined
450 steeply, decreasing by approximately -43% (95% CI -52:-33). There was a positive effect of change in
451 habitat suitability on trends, such that routes with habitat loss had more negative population trends ρ_β =
452 0.025 (95% CI 0.003:0.047). Trends were negative across the species' range, but most negative in the
453 coastal regions where the habitat has changed the most and where the species is also most abundant (left
454 panel, Figure 11, and Figure S7). The change in habitat suitability affected the spatial patterns in trend
455 (Figure 11), with the greater loss of habitat in the coastal regions (Figure S7) accounting for most of the
456 increased rates of decline in the core of the species' range. The residual trend component alone does not
457 show the same coastal-decline pattern (right panel, Figure 11).

458 Annual variation in the number of ponds around BBS routes affected the overall rate of population change
459 in Horned Grebes and showed a spatial relationship (Figure 12). In a model including the annual pond

460 variation, the Horned Grebe population declined overall at a rate of -1.9 %/year from 1975-2017. After
461 removing the effect of annual pond variation, the long-term rate of decline was -2.2 %/year. The effect of
462 annual fluctuations in the number of ponds was positive across the region: the mean value of $\rho' = 0.42$
463 (95% CI 0.29:0.55), but there was also a spatial gradient in intensity. The effect of the number of ponds
464 per year was strongest in the northwest part of the Prairies (Figure 12).

465

Discussion

Spatially explicit, route-level models are useful for visualizing fine spatial patterns at scales more relevant to local conservation, understanding the drivers of population change, and estimating the effects of covariates on relative abundance and trends (e.g., Betts et al. 2022). At this fine spatial scale, incorporating spatial information improves the models' predictions of future data. This improvement is particularly clear for both the iCAR and the GP models, where the spatial models had higher accuracy for out-of-sample predictions than the non-spatial model for almost every species we compared. Fine spatial patterns in trend estimates across a species' range are useful for generating hypotheses on the ecological drivers of population change. Route-level models also allow for the incorporation of local habitat covariates on relative abundance and trend at fine scales, which is important as some covariates affect bird populations at scales much smaller than the strata often used for broad-scale analyses, such as Bird Conservation Regions (BCRs) or states/provinces/territories (Thogmartin et al. 2004, Paton et al. 2019, Monroe et al. 2022). Route-level patterns are also useful in guiding conservation and/or further monitoring efforts, such as identifying small areas for conservation purposes or diverging population trends within management areas (i.e., strata or BCR).

These route-level, spatial models generate smoothed patterns of variation in population trends across a species' range, which will greatly facilitate hypothesis generation and direct investigation to better understand the drivers of population change similar to (Fink et al. 2023b). For example, the spatial models show relatively smooth patterns in Baird's Sparrow trends across the species' range (Figure 4), which are not evident in the simpler, non-spatial model. In the spatial models, Baird's Sparrow has increased in the west and decreased in the eastern portion of its range. This longitudinal pattern may suggest hypotheses related to spatial variation in factors such as climate, or habitat amount, which could then be directly tested by incorporating covariates representing these factors into a subsequent model. Similarly, the complex spatial patterns in the trends of Hairy Woodpecker (*Dryobates villosus*, Figure 8) show some latitudinal variation in trends in the west that is not as clear in the east, suggesting that there

may be distinct processes related to latitude driving trends in these two regions. Comparisons of these patterns among species may be particularly informative. For example, the similar southeast to northwest gradients in trends for Canyon Towhee and Western Bluebird may suggest some similarity in the underlying drivers of population change (Figure 9). These observations illustrate the types of hypothesis-generating that these fine-scale, spatially explicit models can help generate.

All three of the spatial models (iCAR, GP, and BYM) generated broadly similar spatial patterns in route-level trends for the subset of species we compared (Figure 5 and Figure S2). For the species in this study, there is little support for the extra variation in route-level trends in the BYM model, given it had lower predictive accuracy than the simpler iCAR model in all cases. The iCAR structure outperformed the GP models for 31% of the species and is more computationally efficient. Overall, the GP model outperformed the iCAR model for most (69%) of the species we compared. The GP model also produces smoother spatial patterns in population trends than the other spatial models and for some, the difference is striking (e.g. Black-throated Gray Warbler *Setophaga nigrescens*, California Quail *Callipepla californica,* and the Golden-winged Warbler *Vermivora chrysoptera* in Figure S3). For the first two species, the GP outperformed the iCAR for accuracy, while for the third species, the iCAR was better (Figure S4).

Though the GP model had better predictive accuracy for most species, the best spatial structure to use will depend on the species and the goals of a given study. Until GP models become more efficient to implement (Hoffmann and Onnela 2023), the iCAR structure may be preferable for larger datasets (e.g., broad-ranging species and or longer time-series). The iCAR structure may also provide more direct control to model discontinuities in the spatial relationships, such as complex range boundaries (Ver Hoef et al. 2018, Pebesma and Bivand 2023), since there are many ways to define neighborhood relationships (Freni-Sterrantino et al. 2018). A species with limited dispersal may be particularly sensitive to the Euclidean distance between points and therefore better modeled with the GP, but the simplification of space using the iCAR structure may be sufficient for most wide-ranging migratory birds. For example, for some species, there are routes that are separated from most other routes by relatively large distances.

These “isolated” routes are treated very differently by the iCAR and GP models: they are considered close neighbors in the iCAR model regardless of the distance between them, whereas in the GP model, the large distance between routes reduces their correlation with their nearest neighbors. Interestingly, when we compared the predictive accuracy between the GP and iCAR models for routes where the nearest neighboring route where the species was detected > 200km away, the iCAR tended to outperform the GP (Figure S8). Therefore, a more accurate representation of the long distances separating these isolated routes in the GP model does not necessarily result in more accurate predictions, and when combined with the GP’s computational load, it may be more effective to treat space as a series of relative spatial relationships using the iCAR structure.

These route-level BBS models provide many opportunities for further comparisons, applications, and elaborations. Fine-scale estimates could be summarized across species and within regions, such as summaries of the spatial patterns in grassland bird trends or summaries for a given species within BCRs or states/provinces/territories and compared to estimates from models fit at those broader spatial scales. The spatial patterns in trend estimates also allow for comparison of BBS data to other fine-grained maps of species trend and relative abundance, such as eBird (Sullivan et al. 2014, Fink et al. 2023a) or the Integrated Monitoring in Bird Conservation Regions (IMBCR) program (Pavlacky et al. 2017). Comparison of trend estimates between the two programs for the same species and periods of time could provide useful validation of and or help understand differences between the two sources of information. Similarly, there are many possible avenues to integrate information across programs for a given period (e.g., recent trends) or through time (e.g., long-term information from the BBS with more recent information from eBird and/or IMBCR). Through data integration, we can overcome some of the limitations of the BBS, such as the lack of detectability data (Edwards et al. 2023a) , and road-side survey, while retaining the program’s benefits of a long time-series with a structured spatial design and consistent sampling through time.

Separating the route-level intercepts from the observer-level intercepts allows us to better model patterns in relative abundance. It should also allow for improved modeling of the variation among observers. Although many previous BBS analyses have combined observer and route effects (Link et al. 2020, Smith and Edwards 2020), doing so contributes some of the variation in relative abundance among routes to observer variation, which is effectively sampling noise. The model will struggle to separately estimate intercepts for observers and routes in situations where there are few data to inform the estimates (e.g., cases where a route has only been surveyed by one observer). However, we suggest that if a model has sufficient data to estimate these parameters separately, however weakly, it is preferable to a model that does not separate the variation in relative abundance between routes from the sampling noise of observer variation. This separation of the observer from route effects is improved by the hierarchical structure of the models, inclusion of spatial information, weakly informative priors, and the improved efficiency of HMC algorithms over the earlier Gibbs sampling algorithms. Although we were motivated by our desire to directly model route-level relative abundance, this approach is equally applicable to other BBS analyses (Smith et al. 2023), at any scale, and is included in the models in the R-package bbsBayes2 (Edwards et al. 2023b).

In both covariate examples, incorporating spatial covariates into the trend analyses tested hypotheses related to the drivers of population change and helped identify specific areas for further research and conservation action. For the Rufous Hummingbird, the model shows higher mean relative abundance on routes with higher habitat suitability and positive effects of the change in habitat suitability on the species' trend (more negative trends on routes where habitat has decreased). These example findings coincide with a recent study which found that the survival rate of rufous hummingbirds was negatively affected by high human population density (English et al. 2024), where there is likely less habitat. Interestingly, it also shows that during this period, the variation among routes in habitat change does not account for all of the decline in the species' population (Figure 11, and Figure S7), suggesting that factors other than local habitat or factors acting outside of the breeding range may be driving the overall decline.

However, covariates other than habitat suitability could represent local habitat better for the Rufous Hummingbird and could result in a different relationship between local habitat and relative abundance. For the Horned Grebe, the effect of annual fluctuations in available wetland habitat (the number of ponds) is positive overall and varies in magnitude across the species' range. The effect is strongest in the western prairies where the effects of drought are often strongest (Johnson et al. 2005, Millett et al. 2009, Roy 2015). These results highlight the importance of continued investment in wetland conservation programs for waterbird populations breeding in the Prairie Potholes Region, and the vulnerability of these species to climate change since their breeding habitat is highly sensitive to climatic conditions.

The structure of the BBS, designed for monitoring temporal changes in bird populations, allows for the efficient estimation of fine-scale patterns in trends and the effects of local drivers of those trends, provided the survey design and the model sufficiently account for potential changes in detectability. Unmodeled changes in detectability of birds through time could explain some of the spatial patterns in trends from these models, if the changes in detectability were coincident across many BBS routes in a particular region. For example, changes in vegetation that affect detectability, such as forest loss adjacent to the roads where surveys occur, could bias estimates of trends from BBS observations or bias estimates of the effects of that changing vegetation on bird populations. The BBS field methods control for many factors that are known to affect detectability, including weather, season, time of day, and among observer variation. Other potential sources of bias in BBS trends include changes in phenology, changes in traffic during surveys, among observer variation, and within observer variation, although so far each of these when studied have be shown to have minor effects on trend estimates (Kendall et al. 1996, Griffith et al. 2010, English et al. 2021), or can be statistically adjusted in the models (Sauer et al. 1994). There is ongoing work to further explore the potential bias in trends due to observer aging (Farmer et al. 2014, U.S. Geological Survey and Canadian Wildlife Service 2020). The models here could also be modified to integrate BBS observations with additional data that could support adjustments for possible changes in

589 detectability (e.g., (Edwards et al. 2023a)), or additional data that could directly estimate changes in
590 detectability through time (Pavlacky et al. 2017, Zhao et al. n.d.).

591 Fine-scale models can also be used to inform different scales of decisions and communities. Decisions on
592 land use for industries such as agriculture, forestry, and housing are often made at fine scales (Sodhi et al.
593 2011, Malek et al. 2019). Likewise, habitat protection and restoration by community organizations,
594 municipal governments, and non-governmental organizations occur at fine scales (Sheppard 2005,
595 Aronson et al. 2017). For example, the Horned Grebe covariate analysis confirms the vulnerability of
596 waterbird species in the northwestern Prairie Potholes Region and supports a current initiative to protect
597 critical shallow wetlands in the region (Prairie Habitat Joint Venture 2020). Community support is
598 important for the success of conservation initiatives (Berkes 2004, Bennett and Dearden 2014), and so
599 providing estimates at scales relevant to communities may increase community support for conservation
600 and encourage a feeling of stewardship. Further, routes are a relevant scale for the volunteer observers
601 dedicated to the BBS, with the average BBS volunteer participating for 12 years. Producing estimates at a
602 route-level allows volunteers' to see the direct results of their efforts over the years, a large motivator for
603 many citizen science volunteers (Phillips et al. 2019).

604 We hope that the models and examples here will facilitate greater use of the BBS data, providing new
605 ways to explore the spatiotemporal patterns in relative abundance and trends, and new tools with which to
606 better understand the drivers of those patterns. The long-term information from the BBS provides a
607 priceless benchmark against which to calibrate an otherwise shifting ecological baseline. In addition to its
608 monitoring role, the structured design of the BBS also provides excellent data to study the drivers and
609 correlates of population change using tractable and interpretable models such as these.

610

References Cited

Aronson, M. F., C. A. Lepczyk, K. L. Evans, M. A. Goddard, S. B. Lerman, J. S. MacIvor, C. H. Nilon, and T. Vargo (2017). Biodiversity in the city: key challenges for urban green space management. Frontiers in Ecology and the Environment 15:189–196.

Barnett, L. A. K., E. J. Ward, and S. C. Anderson (2021). Improving estimates of species distribution change by incorporating local trends. Ecography 44:427–439.

Bennett, N. J., and P. Dearden (2014). Why local people do not support conservation: Community perceptions of marine protected area livelihood impacts, governance and management in Thailand. Marine Policy 44:107–116.

Berkes, F. (2004). Rethinking Community-Based Conservation. Conservation Biology 18:621–630.

Besag, J., and C. Kooperberg (1995). On conditional and intrinsic autoregressions. Biometrika 82:733–746.

Besag, J., J. York, and A. Mollié (1991). Bayesian image restoration, with two applications in spatial statistics. Annals of the Institute of Statistical Mathematics 43:1–20.

Betts, M. G., Z. Yang, A. S. Hadley, A. C. Smith, J. S. Rousseau, J. M. Northrup, J. J. Nocera, N. Gorelick, and B. D. Gerber (2022). Forest degradation drives widespread avian habitat and population declines. Nature Ecology & Evolution 6:709–719.

Bird Studies Canada, and North American Bird Conservation Initiative (2014). Bird Conservation Regions. [Online.] Available at https://birdscanada.org/bird-science/nabci-bird-conservation-regions.

Bled, F., J. Sauer, K. Pardieck, P. Doherty, and J. A. Royle (2013). Modeling Trends from North American Breeding Bird Survey Data: A Spatially Explicit Approach. PLoS ONE 8:e81867.

Buckland, S. T., K. B. Newman, L. Thomas, and N. B. Koesters (2004). State-space models for the dynamics of wild animal populations. Ecological Modelling 171:157–175.

Bürkner, P.-C., J. Gabry, and A. Vehtari (2020). Approximate leave-future-out cross-validation for Bayesian time series models. Journal of Statistical Computation and Simulation 90:2499–2523.

CEC (1997). Ecological Regions of North America: Toward a Common Perspective. Commission for Environmental Cooperation. Montréal, QC, Canada.

Cressie, N., C. A. Calder, J. S. Clark, J. M. V. Hoef, and C. K. Wikle (2009). Accounting for uncertainty in ecological analysis: the strengths and limitations of hierarchical statistical modeling. Ecological Applications 19:553–570.

Doser, J. W., M. Kéry, S. P. Saunders, A. O. Finley, B. L. Bateman, J. Grand, S. Reault, A. S. Weed, and E. F. Zipkin (2024). Guidelines for the use of spatially varying coefficients in species distribution models. Global Ecology and Biogeography 33:e13814.

Drever, M. C., A. C. Smith, L. A. Venier, D. J. H. Sleep, and D. A. MacLean (2018). Cross-scale effects of spruce budworm outbreaks on boreal warblers in eastern Canada. Ecology and Evolution 8:7334–7345.

Edwards, B. P. M., and A. C. Smith (2021). bbsBayes: An R Package for Hierarchical Bayesian Analysis of North American Breeding Bird Survey Data. Journal of Open Research Software 9:19.

Edwards, B. P. M., A. C. Smith, T. D. S. Docherty, M. A. Gahbauer, C. R. Gillespie, A. R. Grinde, T. Harmer, D. T. Iles, S. M. Matsuoka, N. L. Michel, A. Murray, et al. (2023a). Point count offsets for estimating population sizes of north American landbirds. Ibis 165:482–503.

Edwards, B. P. M., A. C. Smith, and S. LaZerte (2023b). bbsBayes2: Hierarchical Bayesian Analysis of North American BBS Data. [Online.] Available at https://github.com/bbsBayes/bbsBayes2.

English, S. G., C. A. Bishop, S. Wilson, and A. C. Smith (2021). Current contrasting population trends among North American hummingbirds. Scientific Reports 11:18369.

English, S. G., S. Wilson, Q. Zhao, C. A. Bishop, and A. J. Moran (2024). Demographic mechanisms and anthropogenic drivers of contrasting population dynamics of hummingbirds. Biological Conservation 289:110415.

Farmer, R. G., M. L. Leonard, J. E. Mills Flemming, and S. C. Anderson (2014). Observer aging and long-term avian survey data quality. Ecology and Evolution 4:2563–2576.

Fink, D., T. Auer, A. Johnson, M. Strimas-Mackey, S. Ligocki, O. Robinson, W. Hochachka, L. Jaromczyk, C. Crowley, K. Dunham, A. Stillman, et al. (2023a). eBird Status and Trends, Data Version: 2022; Released: 2023. *Cornell Lab of Ornithology, Ithaca, New York*. [Online.] Available at https://science.ebird.org/status-and-trends/species/lessca/abundance-map.

Fink, D., A. Johnston, M. Strimas-Mackey, T. Auer, W. M. Hochachka, S. Ligocki, L. Oldham Jaromczyk, O. Robinson, C. Wood, S. Kelling, and A. D. Rodewald (2023b). A Double machine learning trend model for citizen science data. Methods in Ecology and Evolution 14:2435–2448.

Freni-Sterrantino, A., M. Ventrucci, and H. Rue (2018). A note on intrinsic conditional autoregressive models for disconnected graphs. Spatial and Spatio-temporal Epidemiology 26:25–34.

Gelman, A., J. Carlin B., H. S. Stern, D. Dunson B., A. Vehtari, and D. Rubin B. (2013). Bayesian Data Analysis. 3rd edition. Chapman and Hall/CRC.

Gelman, A., J. Hwang, and A. Vehtari (2014). Understanding predictive information criteria for Bayesian models. Statistics and Computing 24:997–1016.

Golding, N., and B. V. Purse (2016). Fast and flexible Bayesian species distribution modelling using Gaussian processes. Methods in Ecology and Evolution 7:598–608.

Gombin, J. (2023). Concaveman package. [Online.] Available at https://github.com/joelgombin/concaveman.

Government of Canada (2010). Cosewic / Cosepac - Definitions associated with quantitative criteria. [Online.] Available at https://www.cosewic.ca/index.php/en-ca/assessment-process/wildlife-species-assessment-process-categories-guidelines/quantitative-criteria-definitions.html.

Griffith, E. H., J. R. Sauer, and J. A. Royle (2010). Traffic Effects on Bird Counts on North American Breeding Bird Survey Routes. The Auk 127:387–393.

Hoffmann, T., and J.-P. Onnela (2023). Scalable Gaussian Process Inference with Stan. [Online.] Available at http://arxiv.org/abs/2301.08836.

Hudson, M.-A. R., C. M. Francis, K. J. Campbell, C. M. Downes, A. C. Smith, and K. L. Pardieck (2017). The role of the North American Breeding Bird Survey in conservation. The Condor 119:526–545.

IUCN (2012). IUCN Red List Categories and Criteria: Version 3.1. 2nd edition. IUCN, Gland, Switzerland and Cambridge, UK.

Jefferys, K. M., M. G. Betts, W. D. Robinson, J. R. F. Curtis, T. A. Hallman, A. C. Smith, C. Strevens, and J. Aguirre-Gutiérrez (2024). Breeding habitat loss linked to declines in Rufous Hummingbirds. Avian Conservation and Ecology 19.

Johnson, W. C., B. V. Millett, T. Gilmanov, R. A. Voldseth, G. R. Guntenspergen, and D. E. Naugle (2005). Vulnerability of Northern Prairie Wetlands to Climate Change. BioScience 55:863–872.

Kendall, W. L., B. G. Peterjohn, and J. R. Sauer (1996). First-Time Observer Effects in the North American Breeding Bird Survey. The Auk 113:823–829.

Kruschke, J. K. (2015). Doing Bayesian data analysis: a tutorial with R, JAGS, and Stan. Edition 2. Academic Press, Boston.

Link, W. A., and J. R. Sauer (1997). New Approaches to the Analysis of Population Trends in Land Birds: Comment. Ecology 78:2632–2634.

Link, W. A., and J. R. Sauer (2016). Bayesian cross-validation for model evaluation and selection, with application to the North American Breeding Bird Survey. Ecology 97:1746–1758.

Link, W. A., J. R. Sauer, and D. K. Niven (2020). Model selection for the North American Breeding Bird Survey. Ecological Applications 30:e02137.

Malek, Ž., B. Douw, J. V. Vliet, E. H. V. D. Zanden, and P. H. Verburg (2019). Local land-use decision-making in a global context. Environmental Research Letters 14:083006.

McElreath, R. (2023). rethinking. [Online.] Available at https://github.com/rmcelreath/rethinking.

Meehan, T. D., N. L. Michel, and H. Rue (2019). Spatial modeling of Audubon Christmas Bird Counts reveals fine-scale patterns and drivers of relative abundance trends. Ecosphere 10:e02707.

Millett, B., W. C. Johnson, and G. Guntenspergen (2009). Climate trends of the North American prairie pothole region 1906–2000. Climatic Change 93:243–267.

Mirochnitchenko, N. A., E. F. Stuber, and J. J. Fontaine (2021). Biodiversity scale-dependence and opposing multi-level correlations underlie differences among taxonomic, phylogenetic and functional diversity. Journal of Biogeography 48:2989–3003.

Monroe, A. P., J. A. Heinrichs, A. L. Whipple, M. S. O'Donnell, D. R. Edmunds, and C. L. Aldridge (2022). Spatial scale selection for informing species conservation in a changing landscape. Ecosphere 13:e4320.

718 Morris, M., K. Wheeler-Martin, D. Simpson, S. J. Mooney, A. Gelman, and C. DiMaggio (2019).
719 Bayesian hierarchical spatial models: Implementing the Besag York Mollié model in stan. Spatial
720 and Spatio-temporal Epidemiology 31:100301.

721 Morrison, C. A., R. A. Robinson, J. A. Clark, and J. A. Gill (2010). Spatial and temporal variation in
722 population trends in a long-distance migratory bird. Diversity and Distributions 16:620–627.

723 North American Bird Conservation Initiative (2022). The State of the Birds, United States of America.

724 North American Bird Conservation Initiative Canada (2019). The State of Canada's Birds, 2019.
725 Environment and Climate Change Canada.

726 Paton, G. D., A. V. Shoffner, A. M. Wilson, and S. A. Gagné (2019). The traits that predict the magnitude
727 and spatial scale of forest bird responses to urbanization intensity. PLOS ONE 14:e0220120.

728 Pavlacky, D. C., P. M. Lukacs, J. A. Blakesley, R. C. Skorkowsky, D. S. Klute, B. A. Hahn, V. J. Dreitz,
729 T. L. George, and D. J. Hanni (2017). A statistically rigorous sampling design to integrate avian
730 monitoring and management within Bird Conservation Regions. PLOS ONE 12:e0185924.

731 Pebesma, E. (2018). Simple Features for R: Standardized Support for Spatial Vector Data. The R Journal
732 10:439–446.

733 Pebesma, E., and R. Bivand (2023). Spatial Data Science: With Applications in R. 1st edition. Chapman
734 and Hall/CRC, Boca Raton.

735 Phillips, T. B., H. L. Ballard, B. V. Lewenstein, and R. Bonney (2019). Engagement in science through
736 citizen science: Moving beyond data collection. Science Education 103:665–690.

737 Prairie Habitat Joint Venture (2020). Prairie Habitat Joint Venture: The Prairie Parklands
738 Implemenetation Plan 2013-2020. [Online.] Available at https://www.phjv.ca/wp-
739 content/uploads/2020/12/PHJV-Implemenetation-Plan-PRAIRIE-PARKLAND-2013-2020-
740 Final.pdf#page=33.

741 Renfrew, R. B., D. Kim, N. Perlut, J. Smith, J. Fox, and P. P. Marra (2013). Phenological matching across
742 hemispheres in a long-distance migratory bird. Diversity and Distributions 19:1008–1019.

743 Roberts, D. R., V. Bahn, S. Ciuti, M. S. Boyce, J. Elith, G. Guillera-Arroita, S. Hauenstein, J. J. Lahoz-
744 Monfort, B. Schröder, W. Thuiller, D. I. Warton, et al. (2017). Cross-validation strategies for data
745 with temporal, spatial, hierarchical, or phylogenetic structure. Ecography 40:913–929.

746 Rosenberg, K. V., P. J. Blancher, J. C. Stanton, and A. O. Panjabi (2017). Use of North American
747 Breeding Bird Survey data in avian conservation assessments. The Condor 119:594–606.

748 Rosenberg, K. V., A. M. Dokter, P. J. Blancher, J. R. Sauer, A. C. Smith, P. A. Smith, J. C. Stanton, A.
749 Panjabi, L. Helft, M. Parr, and P. P. Marra (2019). Decline of the North American avifauna.
750 Science 366:120–124.

751 Roy, C. (2015). Quantifying Geographic Variation in the Climatic Drivers of Midcontinent Wetlands with
752 a Spatially Varying Coefficient Model. PLOS ONE 10:e0126961.

753 Sauer, J. R., J. E. Fallon, and R. Johnson (2003). Use of North American Breeding Bird Survey Data to
754 Estimate Population Change for Bird Conservation Regions. The Journal of Wildlife
755 Management 67:372–389.

756 Sauer, J. R., and W. A. Link (2011). Analysis of the North American Breeding Bird Survey Using
757 Hierarchical Models. The Auk 128:87–98.

758 Sauer, J. R., K. L. Pardieck, D. J. Ziolkowski, A. C. Smith, M.-A. R. Hudson, V. Rodriguez, H. Berlanga,
759 D. K. Niven, and W. A. Link (2017). The first 50 years of the North American Breeding Bird
760 Survey. The Condor 119:576–593.

761 Sauer, J. R., B. G. Peterjohn, and W. A. Link (1994). Observer Differences in the North American
762 Breeding Bird Survey. The Auk 111:50–62.

763 Sheppard, S. R. (2005). Participatory decision support for sustainable forest management: a framework
764 for planning with local communities at the landscape level in Canada. Canadian Journal of Forest
765 Research 35:1515–1526.

766 Smith, A. C., A. D. Binley, L. Daly, B. P. M. Edwards, D. Ethier, B. Frei, D. Iles, T. D. Meehan, N. L.
767 Michel, and P. A. Smith (2024). Spatially explicit Bayesian hierarchical models improve
768 estimates of avian population status and trends. Ornithological Applications 126:duad056.

769 Smith, A. C., and B. P. M. Edwards (2021). North American Breeding Bird Survey status and trend
770 estimates to inform a wide range of conservation needs, using a flexible Bayesian hierarchical
771 generalized additive model. The Condor 123:duaa065.

772 Smith, A. C., M.-A. R. Hudson, C. Downes, and C. M. Francis (2014). Estimating breeding bird survey
773 trends and annual indices for Canada: how do the new hierarchical Bayesian estimates differ from
774 previous estimates? The Canadian Field-Naturalist 128:119–134.

775 Smith, G. W. (1995). A Critical Review of the Aerial and Ground Surveys of Breeding Waterfowl in
776 North America. U.S. Department of the Interior, National Biological Service.

777 Sodhi, N. S., R. Butler, W. F. Laurance, and L. Gibson (2011). Conservation successes at micro-, meso-
778 and macroscales. Trends in Ecology & Evolution 26:585–594.

779 Sorenson, L. G., R. Goldberg, T. L. Root, and M. G. Anderson (1998). Potential Effects of Global
780 Warming on Waterfowl Populations Breeding in the Northern Great Plains. Climatic Change
781 40:343–369.

782 Stanton, R. L., C. A. Morrissey, and R. G. Clark (2018). Analysis of trends and agricultural drivers of
783 farmland bird declines in North America: A review. Agriculture, Ecosystems & Environment
784 254:244–254.

785 Stedman, S. J. (2020). Horned Grebe (Podiceps auritus). In Birds of the World (S. M. Billerman, B. K.
786 Keeney, P. G. Rodewald and T. S. Schulenberg, Editors). Cornell Lab of Ornithology.

787 Steen, V. A., S. K. Skagen, and C. P. Melcher (2016). Implications of Climate Change for Wetland-
788 Dependent Birds in the Prairie Pothole Region. Wetlands 36:445–459.

Sullivan, B. L., J. L. Aycrigg, J. H. Barry, R. E. Bonney, N. Bruns, C. B. Cooper, T. Damoulas, A. A. Dhondt, T. Dietterich, A. Farnsworth, D. Fink, et al. (2014). The eBird enterprise: An integrated approach to development and application of citizen science. Elsevier 169:31–40.

Thogmartin, W. E., J. R. Sauer, and M. G. Knutson (2004). A Hierarchical Spatial Model of Avian Abundance with Application to Cerulean Warblers. Ecological Applications 14:1766–1779.

Thompson, F. R., and F. A. La Sorte (2008). Comparison of Methods for Estimating Bird Abundance and Trends from Historical Count Data. The Journal of Wildlife Management 72:1674–1682.

Thorson, J. T., C. L. Barnes, S. T. Friedman, J. L. Morano, and M. C. Siple (2023). Spatially varying coefficients can improve parsimony and descriptive power for species distribution models. Ecography 2023:e06510.

U.S. Geological Survey and Canadian Wildlife Service (2020). Strategic Plan for the North American Breeding Bird Survey, 2020–30. U.S. Geological Survey 1466.

Van Wilgenburg, S., E. Beck, B. Obermayer, T. Joyce, and B. Weddle (2015). Biased representation of disturbance rates in the roadside sampling frame in boreal forests: implications for monitoring design. Avian Conservation and Ecology 10.

Veech, J. A., K. L. Pardieck, and D. J. Ziolkowski Jr. (2017). How well do route survey areas represent landscapes at larger spatial extents? An analysis of land cover composition along Breeding Bird Survey routes. The Condor 119:607–615.

Ver Hoef, J. M., E. E. Peterson, M. B. Hooten, E. M. Hanks, and M.-J. Fortin (2018). Spatial autoregressive models for statistical inference from ecological data. Ecological Monographs 88:36–59.

Wilson, S., S. L. LaDeau, A. P. Tøttrup, and P. P. Marra (2011). Range-wide effects of breeding- and nonbreeding-season climate on the abundance of a Neotropical migrant songbird. Ecology 92:1789–1798.

Wilson, S., A. C. Smith, and I. Naujokaitis-Lewis (2018). Opposing responses to drought shape spatial population dynamics of declining grassland birds. Diversity and Distributions 24:1687–1698.

Wright, W. J., K. M. Irvine, T. J. Rodhouse, and A. R. Litt (2021). Spatial Gaussian processes improve multi-species occupancy models when range boundaries are uncertain and nonoverlapping. Ecology and Evolution 11:8516–8527.

Zhao, Q., Q. S. Latif, B. L. Nuse, D. C. Pavlacky Jr., C. L. Kilner, T. B. Ryder, and C. E. Latimer (no date). Integrating counts from rigorous surveys and participatory science to better understand spatiotemporal variation in population processes. Methods in Ecology and Evolution n/a.

Figures and captions

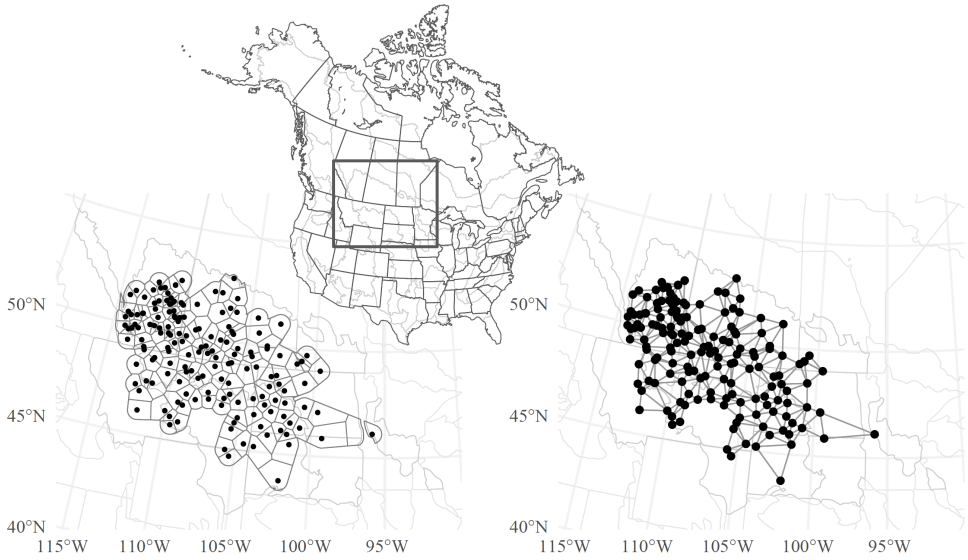

Figure 1. North American Breeding Bird Survey (BBS) route start locations (points in the lower left and lower right images) for routes on which Baird's Sparrow was observed (2006-2021), demonstrating the process used to identify the discrete neighbor relationships for the iCAR and BYM spatial models. The top centre panel shows the full set of standard BBS strata within Canada and the United States. These strata represent the spatial intersection of the countries' states, provinces, and territories (darker grey lines) with the North American Bird Conservation Regions (BCRs lighter grey lines; ecological zones that share similar ecological and climatic features as well as similar bird communities). The dark inset box shows the region highlighted in the lower two panels. The left bottom panel shows the Voronoi tessellated surface used to assign the intervening space to the nearest BBS route start location, the outer edge of this surface is defined by an intersection of a concave polygon surrounding the points and the standard BBS strata where the species occurs. The lower right panel shows routes considered neighbors using lines linking points that share an edge separating their associated Voronoi polygons.

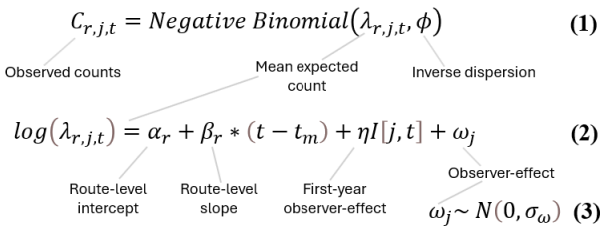

Figure 2. The base model showing the components that are common to all four models. The observed counts (equation 1) for a given species on route-r, by observer-j, in year-t, are realizations of a negative binomial distribution, with mean expected count and inverse dispersion parameter. The log of the mean of the negative binomial distribution was modeled as an additive combination of route-level intercepts, observer-effects, a first-year observer-effect, and route-level slope parameters for the continuous effect of year (t) centered on the mid-year (t_m) of the time-series (equation 2). The observer-effect (random intercept for each observer, equation 3) is a zero-mean normal distribution with an estimated standard deviation. Equation numbers are consistent across Figures 2, 3, and 4.

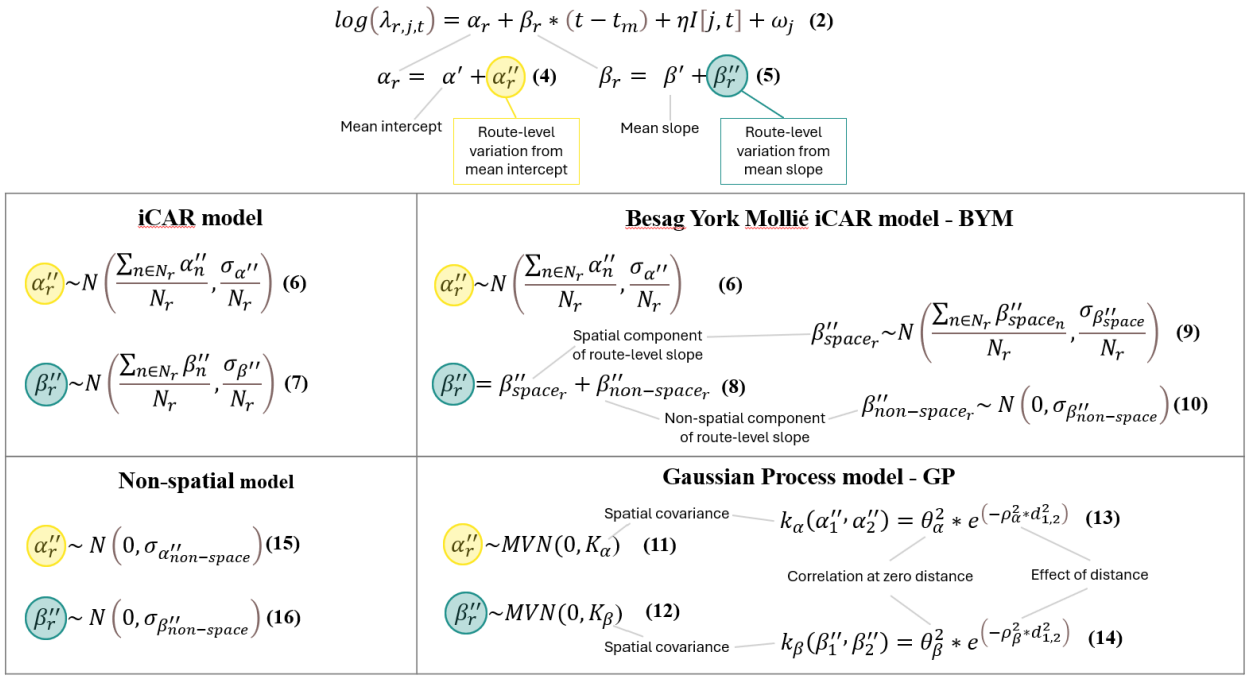

Figure 3. The four spatial models and the components that vary among the models: their treatment of the route-level variation in the intercepts (relative abundance) highlighted in light yellow and route-level variation in slope (trend) highlighted in darker green. All four models use the same base model (equation 2 here and in Figure 2), and all estimate the intercepts independently of the slopes. For each of the models, the intercepts (equation 4) and slopes (equation 5) are additive combinations of a mean and the component that models the route-level variation. In the iCAR model (intrinsic Conditional Autoregressive) and BYM model (Besag York Mollie), the route-level variation from the mean intercept (equation 6) is drawn from a normal distribution centered on the means of the N_r neighboring routes. For the iCAR, the route-level variation in slope on each route (equation 7) was estimated in the same way as the intercepts (a normal distribution centered on the means of the N_r neighboring routes). For the BYM, the route-level variation in slope like the iCAR model (equation 8) but with an additional non-spatial component (equations 9 and 10) as a random effect drawn from a normal distribution. For the GP model, the route-level variation in intercepts and trends (equations 11 and 12) are estimated as zero-mean, multivariate normal distributions (MVN), with covariance matrices estimated using a squared exponential kernel function. The covariance of the parameters among routes is a function of the distance between them modeled by two parameters that control the magnitude of the covariance when distance is zero and the effect of distance (the rate at which covariance decreases with distance, equations 13 and 14). The non-spatial model estimates the route-level variation in intercepts and slopes as independent random effects (equations 15 and 16). Equation numbers are consistent across Figures 2, 3, and 4.

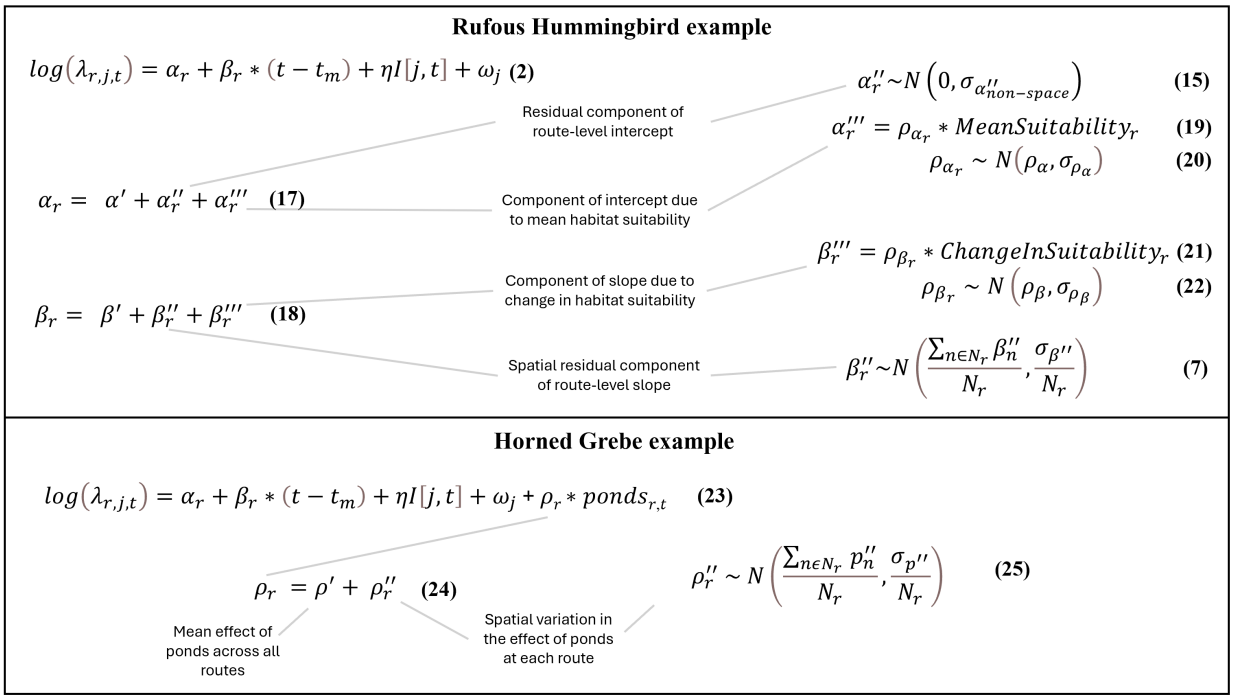

Figure 4. Models used in the two covariate examples. The Rufous Hummingbird example is a modification of the iCAR model where habitat suitability is used as a covariate on route-level slopes and intercepts. Route-level intercepts (equation 17) are the sum of a mean intercept, a non-spatial residual component (equation 15), and a component that is due to the effect of mean habitat suitability (averaged across all years) on each route (equation 19). Route-level slopes (equation 18) are the sum of a mean slope, a spatially varying residual component (equation 7), and a component that is due to the effect of the change in habitat suitability over time on each route (equation 21). The route-specific parameters that estimate the effect of habitat suitability and change in habitat suitability were estimated as normally distributed effects centered on a mean hyperparameter that represents the average effect of the covariate on either the intercept (equation 20) or the slope (equation 22). The Horned Grebe example is a modification of the iCAR model (equation 23) with a spatially varying coefficient (equations 24 and 25) on the effect of the number of ponds surrounding each BBS route in each year on the expected count. The remainder of this model (everything to the left of the pond-effect) is identical to the iCAR model (equations 2, 4, 5, 6, and 7 in Figure 2). Equation numbers are consistent across Figures 2, 3, and 4.

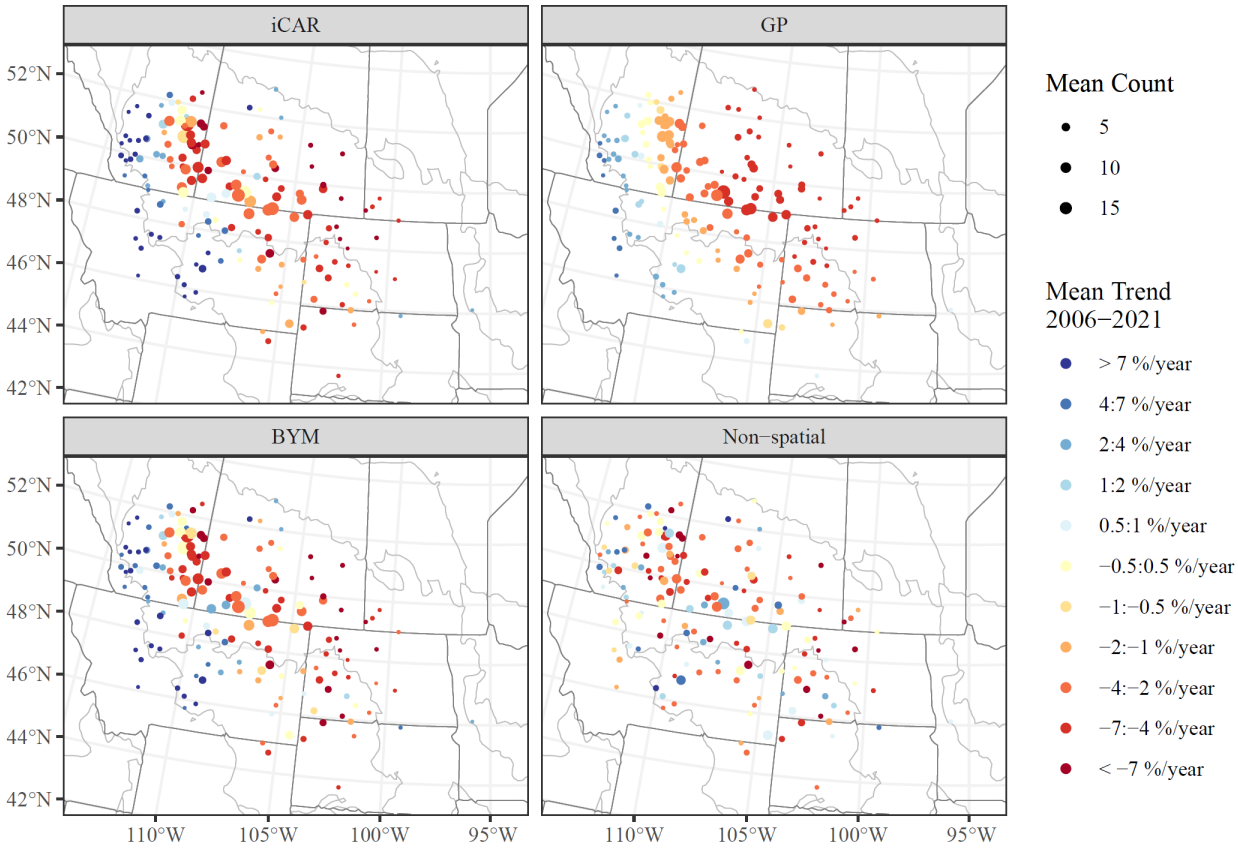

Figure 5. Estimates of trend (colors) and mean relative abundance (size of the points) for Baird's Sparrow populations on BBS routes from 2006-2021, from three spatially explicit models (iCAR, GP, and BYM) and one non-spatial model. Points with warm colors (reds) represent routes with decreasing counts through time, points with cool colors (blues) represent routes with increasing counts through time. The three spatially explicit models suggest very similar spatial patterns in trends, although the GP model suggests smoother spatial variation in trend than either the iCAR or BYM models. Dark grey lines within the maps represent boundaries of state/provinces/territories and the light grey lines represent the boundaries of Bird Conservation Regions. The extents of these map panels are similar to those in figure 1.

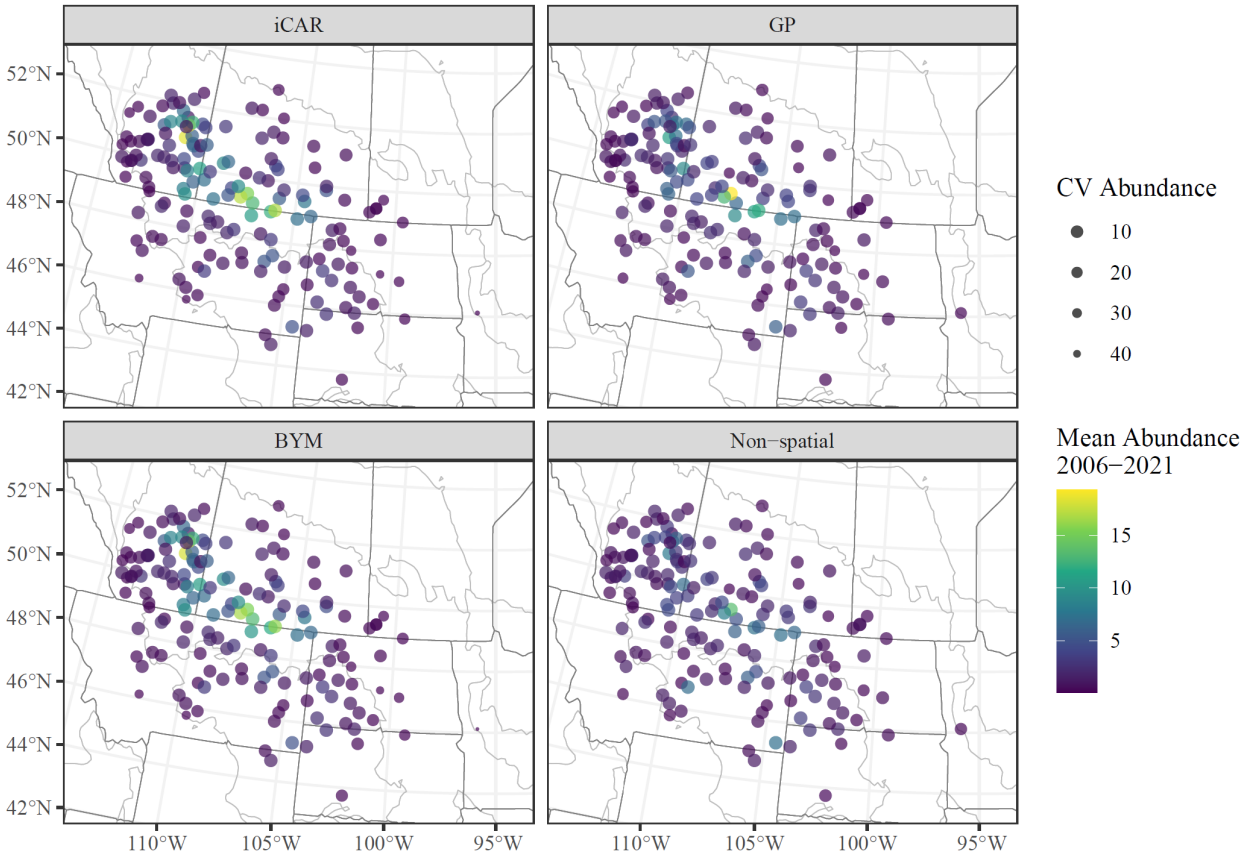

896

897 Figure 6. Estimates of mean relative abundance (colors) and the Coefficient of Variation for the estimates
898 (CV) for Baird's Sparrow populations on BBS routes from 2006-2021, from three spatially explicit
899 models and one non-spatial model. Points with brighter colors (greens and yellows) represent routes with
900 higher estimated mean counts, and points with more precise estimates of abundance (smaller CV) are
901 larger. The iCAR and BYM models estimate almost identical spatial patterns in abundance with a
902 relatively clear peak in the center of the species' range, and relatively smoother spatial variation than
903 either the GP or the non-spatial model. Dark grey lines within the maps represent boundaries of
904 state/provinces/territories and the light grey lines represent the boundaries of Bird Conservation Regions.
905 The extents of these map panels are similar to those in figure 1.

906

907

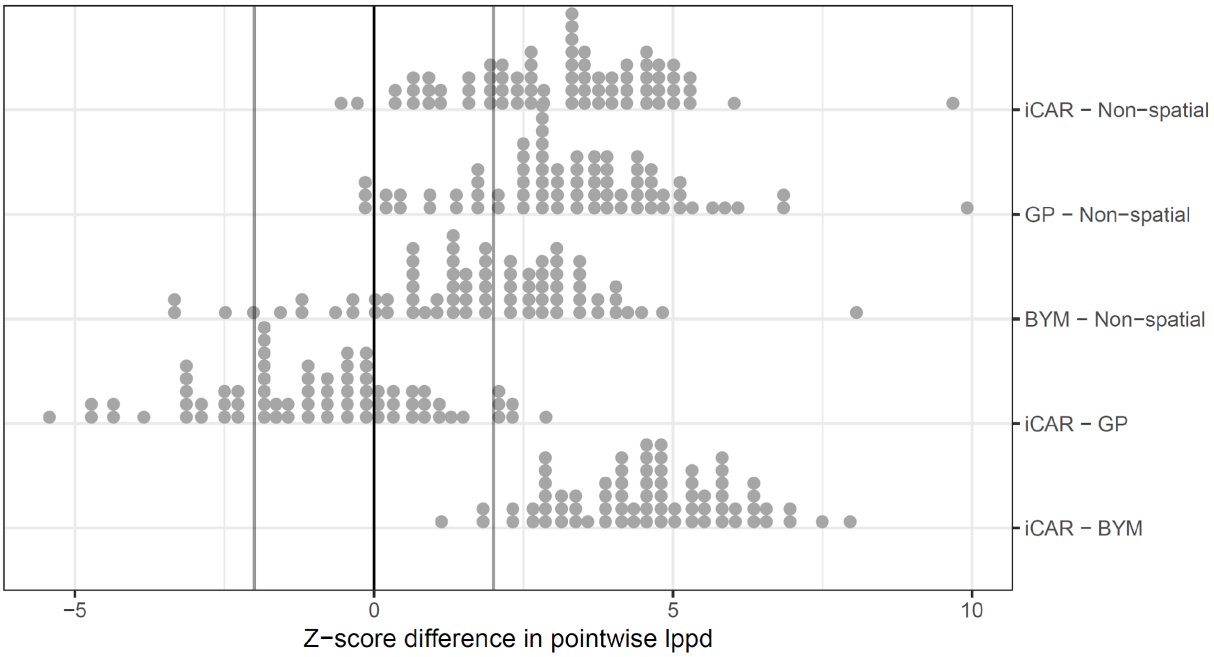

908

909 Figure 7. Leave Future Out (LFO) cross-validation results for 71 small-range species from the North
910 American Breeding Bird Survey (BBS) database, comparing among the four different models. The
911 stacked dot-plots represent species-level summaries of the differences in log posterior predictive density
912 (lppd) between pairs of models. Each point represents one species for a given model comparison. Z-score
913 values on the x-axis represent the difference between the lppd for the two models indicated on the y-axis.
914 Z-scores > 0 (points that fall to the right of the black vertical line) represent species for which the
915 predictive accuracy of the first model is higher than that of the second model (e.g., all but two species in
916 the iCAR vs non-spatial comparison), and vice versa. Z-scores > 2 or < -2 (points that fall to the right or
917 left of the vertical dark gray lines, respectively) represent species for which the mean of the differences
918 between the two models are clear and could be considered "significant" in some statistical frameworks.
919 The top three dot-plots show the comparisons between each of the three spatial models and the non-
920 spatial model. The lower two plots compare the predictive accuracy among the three spatial models and
921 show that the iCAR model out-performs the BYM model for all species, and that the GP model out-
922 performs the iCAR model for some species but not for others. See Figure S4 for species-level details.

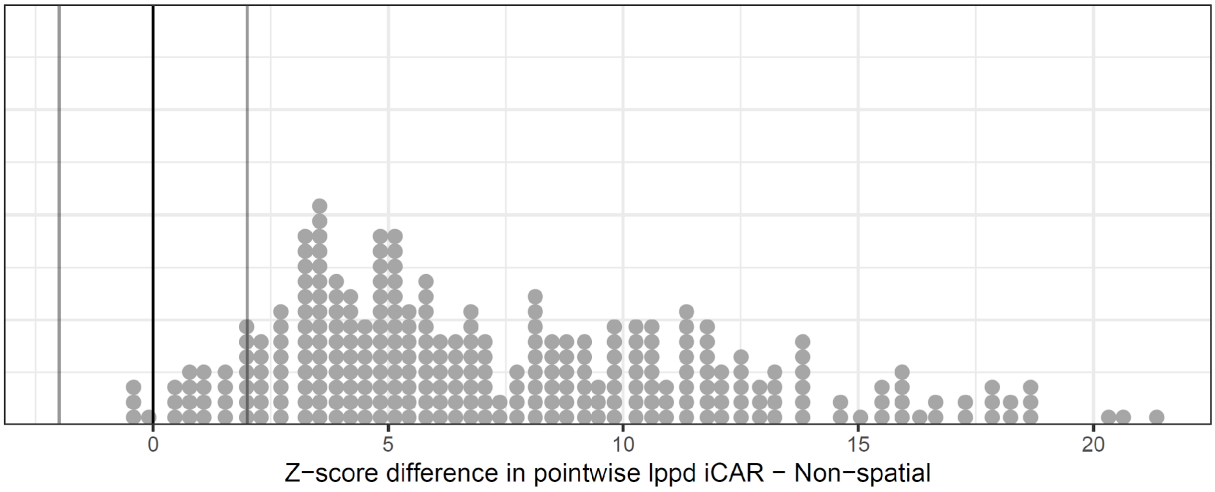

Figure 8. Leave Future Out (LFO) cross-validation results for all 287 species (including the 71 species results in Figure 7) from the North American Breeding Bird Survey (BBS), comparing the iCAR spatial model and the non-spatial model. The stacked dot-plots represent species-level summaries of the differences in log posterior predictive density (lppd) between the two models. Each point represents one species. Z-score values represent the difference between the lppd for the two models accounting for the variation across all counts, and the stacked dots form a histogram. Points that fall to the right of the black vertical line represent species for which the predictive accuracy of the spatial model is higher than that of the non-spatial model. The iCAR spatial model outperforms the non-spatial model for all but four species. For those four species, the predictive accuracy of the two models is very similar (< -1).

933

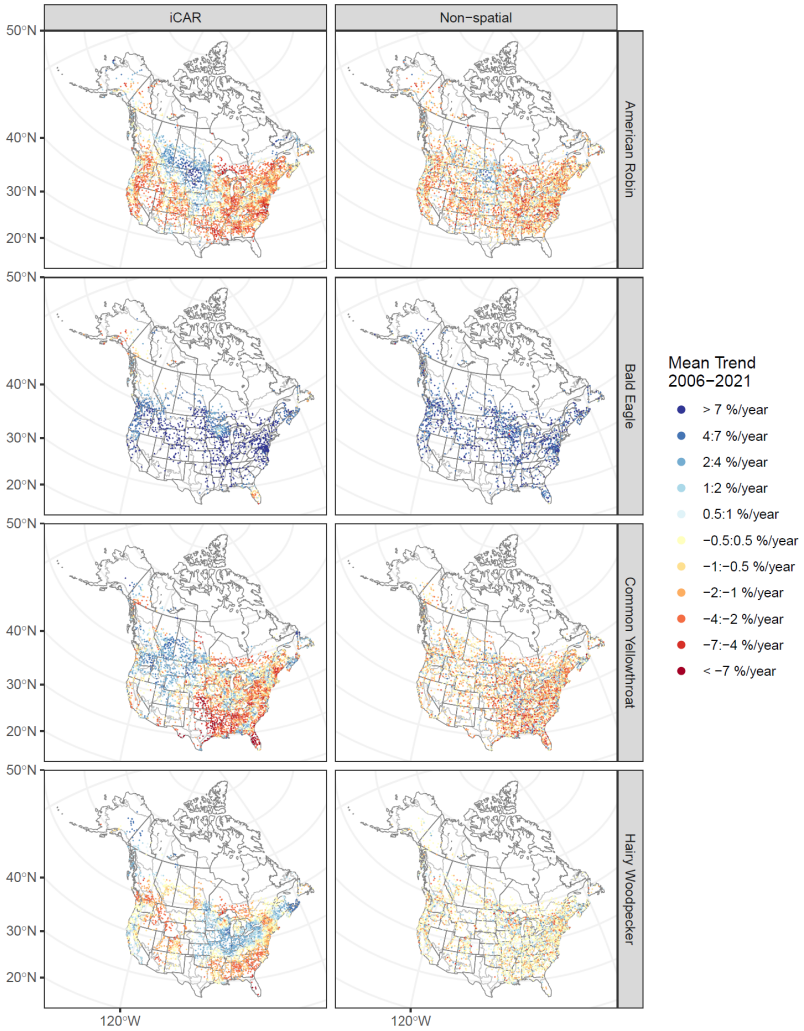

934

935 Figure 9. Examples of the spatial patterns in estimated route-level trends for four broad-range species
936 from an iCAR spatial model (left column) compared to trends estimated from an otherwise identical, non-
937 spatial version of the model (right column). All points are the same size in this plot because the mean
938 abundances vary too much among species to display meaningful variation in this plot. Dark grey lines
939 within the maps represent boundaries of state/provinces/territories in Canada and the United States and
940 the light grey lines represent the boundaries of Bird Conservation Regions.

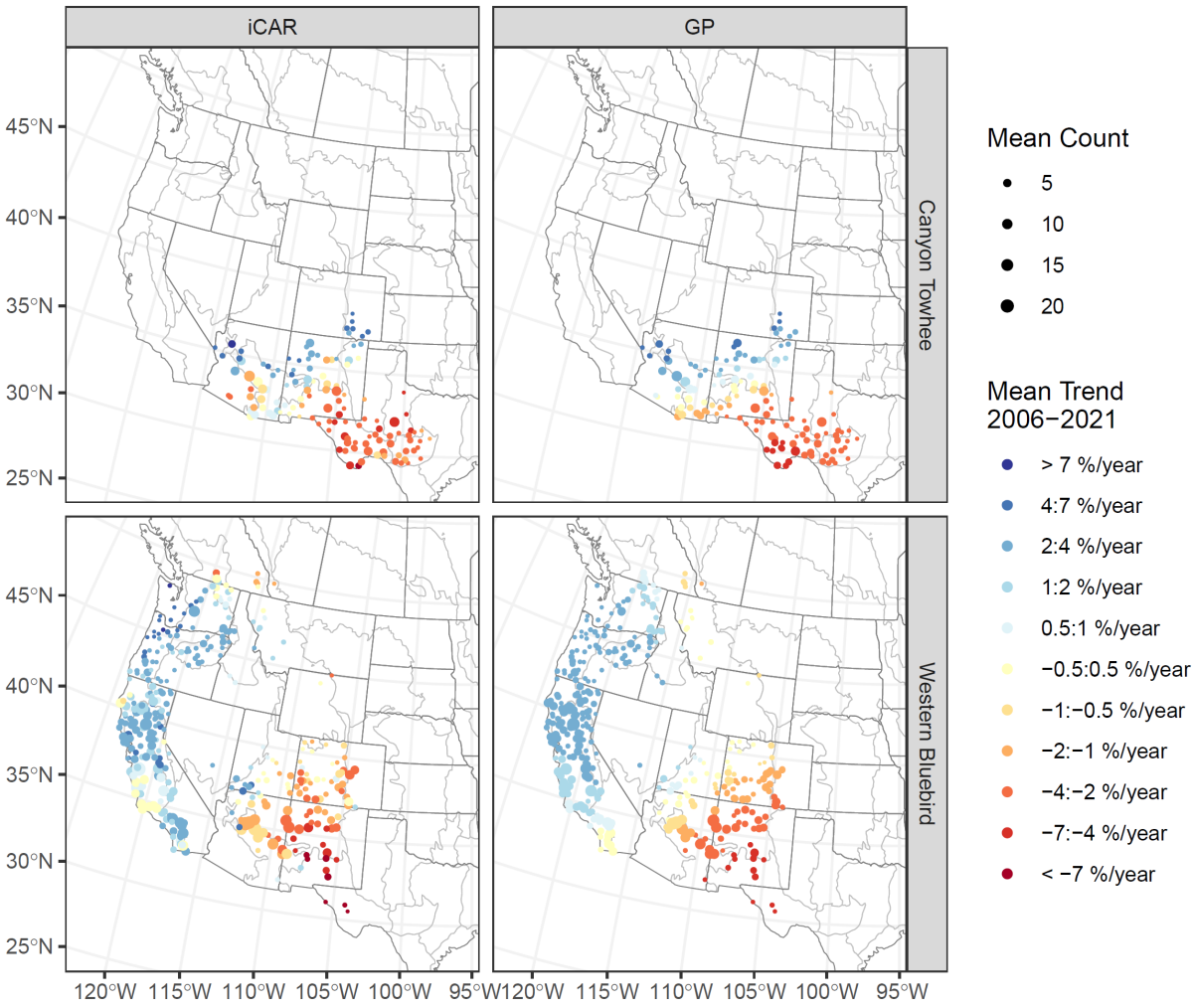

941

942 Figure 10. An example illustrating that the spatial patterns in estimated trends for iCAR and GP models
943 are quite similar, even when one of the models strongly out-performs the other in a cross-validation
944 analysis. For the Canyon Towhee (*Melozone fusca*), the GP model clearly out-performs the iCAR model
945 in predictive accuracy (z-score comparison iCAR – GP = -4.3, left of the center line in Figure 7). For the
946 Western Bluebird (*Sialia mexicana*), the iCAR model out-performs the GP model in predictive accuracy
947 (z-score comparison iCAR – GP = 2.9, right of the center line in Figure 7). Despite the relatively strong
948 difference in predictive accuracy, the spatial patterns are quite similar for both models. All panels in this
949 figure are focused on the western United States and southwestern Canada. Dark grey lines within the
950 maps represent boundaries of state/provinces/territories in Canada and the United States and the light grey
951 lines represent the boundaries of Bird Conservation Regions.

952

953

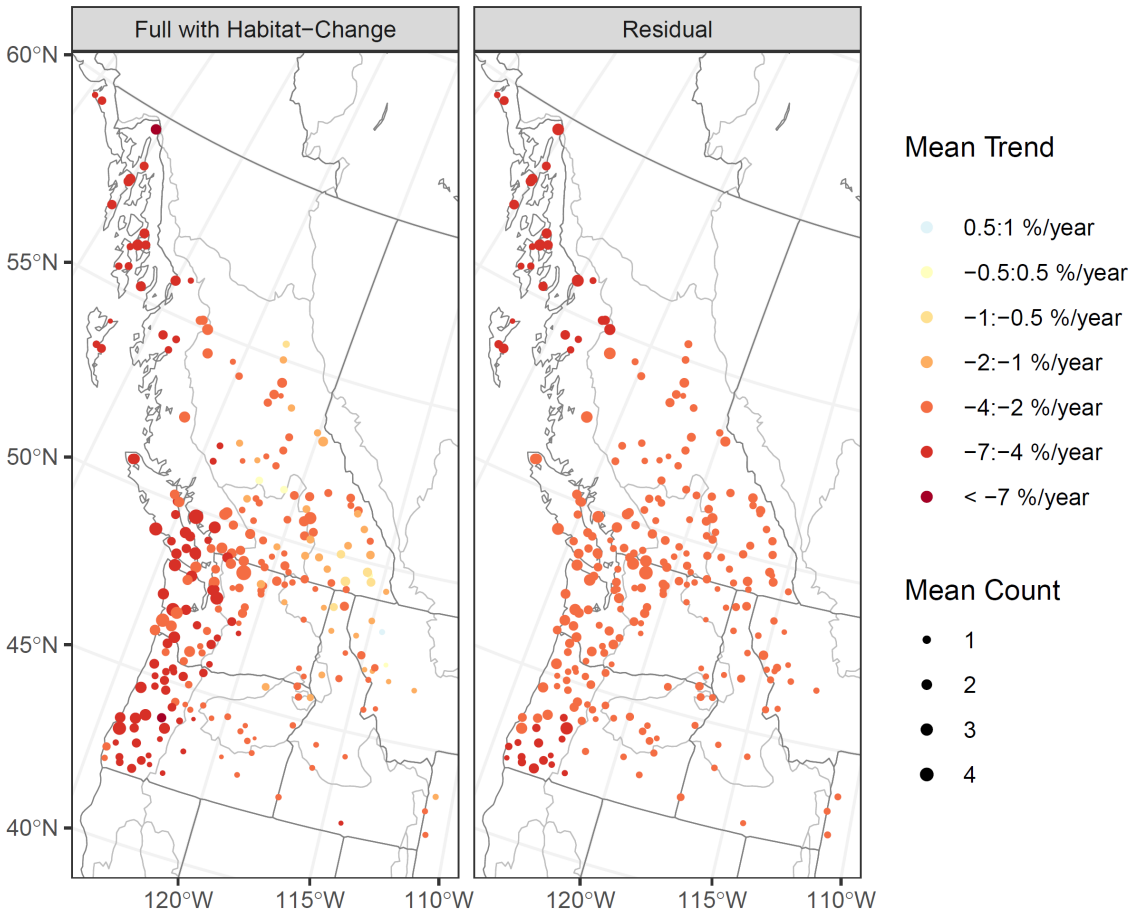

954

955 Figure 11. Map of route-level trend estimates for Rufous Hummingbird (*Selasphorus rufus*) from 2006-
956 2021. The colors represent two sets of trends estimated from the model: "Full with Habitat-Change"
957 represent trends that include the spatially explicit random effects and the effects of local habitat change
958 (left panel) and the "Residual" represent only the residual spatially explicit estimate of trend, after
959 removing the effects of habitat change (right panel). Habitat change appears to be driving most of the
960 variation in trends within the core latitudes of the species range (45°-55° N). The faster rates of decline
961 (darker red) in the western regions and the slower rates of decline (lighter yellow) in the east are evident
962 in the left panel that includes the effects of habitat and are missing from the panel on the right. Dark grey
963 lines within the maps represent boundaries of state/provinces/territories on the West coast of Canada and
964 the United States and the light grey lines represent the boundaries of Bird Conservation Regions.

965

966

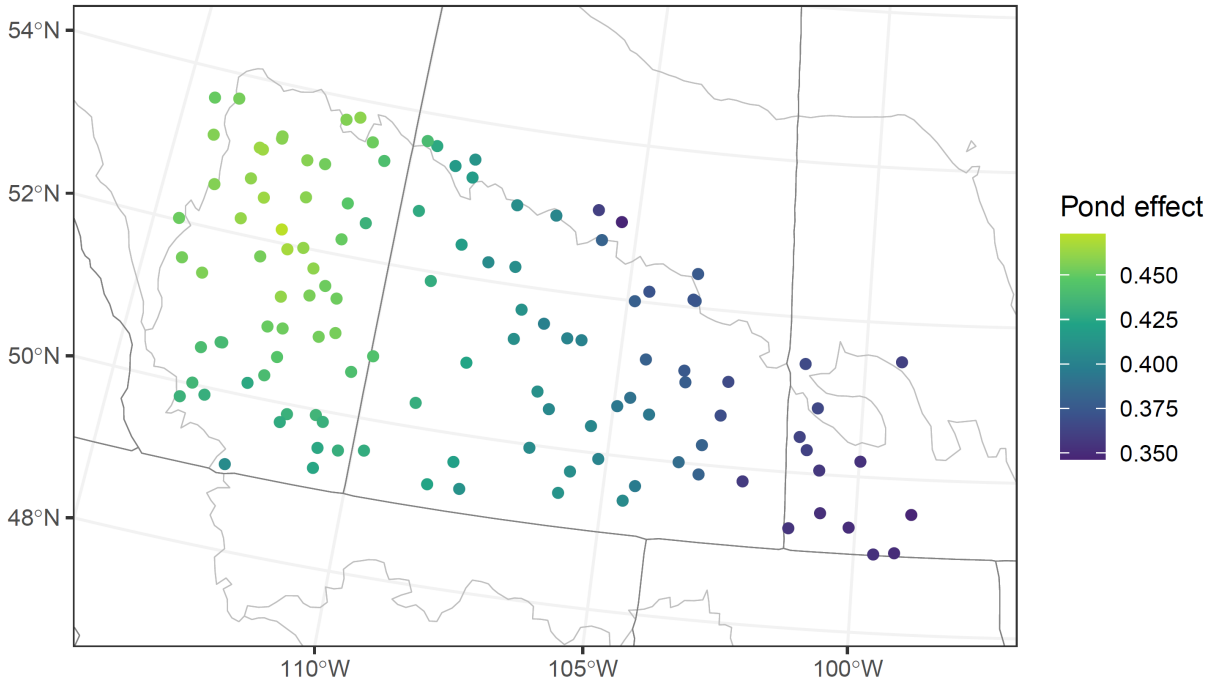

Figure 12. A map of the spatial variation in the effects of annual fluctuations in available habitat (ponds) on the expected counts of Horned Grebe on the North American Breeding Bird Survey (BBS) routes (1975-2017). The pond effect is estimated as a spatially varying coefficient using the iCAR structure among routes and was strongest in the West. Pond effect represents the log-scale effect of annual variation in the number of ponds surrounding a BBS route in a given year on the annual expected count after adjusting for spatially varying long-term trends, observer-effects, and the other parameters included in all of the models we used. Dark grey lines within the maps represent boundaries of state/provinces/territories in the central prairie regions of Canada and the United States (similar extent to Figure 1) and the light grey lines represent the boundaries of Bird Conservation Regions.

Supplements for: Patterns and drivers of population trends on individual Breeding Bird Survey routes using spatially explicit models and route-level covariates.

Contents:

Model Priors

We used weakly informative (Gelman 2006, Lemoine 2019) standard normal priors for the mean species-level intercept and the first-year effect parameter. The mean species-level slope parameter was given a weakly informative normal prior ($\beta' \sim Normal(0, 0.1)$). We consider this prior weakly informative as it reflects our belief that extreme rates of change are unlikely (it places approximately 95% of the prior density for the survey-wide population trends between approximately -20 and +20%/year).

For the iCAR, BYM, and non-spatial models, the priors for the standard deviations of the spatial variation and non-spatial variation of the route-level slopes ($\sigma_{\beta''_{space}}$ and $\sigma_{\beta''_{non-space}}$) had gamma priors with shape = 3 and scale = 30. These gamma priors were weakly informative such that the standard deviation of trends was constrained to more probable scales based on the log-link of the model and to avoid estimates of zero (Chung et al. 2013). Specifically, this gamma prior places the mean of the prior density at approximately 10% per year difference, and 99% of the prior density on the standard deviation of route-level trends at values less than 28% per year difference, while also including a long tail so that the model can estimate more extreme variation, if supported by the data (Chung et al. 2013). The standard deviation of the intercept terms in these models ($\sigma_{\alpha''_{space}}$ and $\sigma_{\alpha''_{non-space}}$) were given a half-normal prior with standard deviation = 2. This weakly informative prior placed most prior density at values < 5, and reflects our belief that across a species' range, mean relative abundance for a fixed survey effort can vary, but is unlikely to vary by more than a few orders of magnitude (Fink et al. 2023). If this relatively wide prior created convergence issues, we re-fit the models with a prior that considered the observed variation in mean counts among routes for a given species. Specifically, we used a half-normal prior with the standard deviation equal to the observed standard deviation of mean log-transformed observed counts among routes. We are confident that this prior is only weakly informative and likely over-estimates the among-route variance because the observed data includes variation among routes, as well as variation among observers.

The parameters of GP models can be quite sensitive to prior distributions (McElreath 2020). We scaled the distance matrix in units of 1000 km and set a half-standard t-distribution prior on θ_α^2 and θ_β^2 with 5 degrees of freedom (Gelman et al. 2013). The half-t prior on θ^2 places most prior density at relatively small values and includes a relatively long tail that allows for larger values, if supported by the data. For most species, we used a weakly informative inverse gamma distribution prior with scale and shape = 5 for ρ_α^2 and ρ_β^2. For some species, the values of ρ^2 failed to converge with this prior, so we set an alternative and more informative prior using a gamma distribution with scale and shape = 2. The

gamma and inverse gamma priors on ρ_α^2 both avoid 0. The weakly informative inverse gamma includes a long right tail that allows the model to estimate spatial dependency that declines steeply with distance (e.g., $\rho_\alpha^2 > 500$ and therefore covariance values near 0 for routes separated by the approximate 40-km length of a BBS route), but for some species, this long tail created convergence difficulties. For these species, we used the gamma prior with a shorter right tail and effectively constrained the estimates of ρ_α^2 to values < 20. This places most of the prior density at values that imply there is some spatial dependency that may extend out to larger distances (500 km – 3000 km).

References

Chung, Y., S. Rabe-Hesketh, V. Dorie, A. Gelman, and J. Liu. 2013. A nondegenerate penalized likelihood estimator for variance parameters in multilevel models. PSYCHOMETRIKA 78:685–709. https://doi.org/10.1007/S11336-013-9328-2.

Fink, D., T. Auer, A. Johnson, M. Strimas-Mackey, S. Ligocki, O. Robinson, W. Hochachka, L. Jaromczyk, C. Crowley, K. Dunham, A. Stillman, I. Davies, A. Rodewald, V. Ruiz-Gutierrez, and C. Wood. 2023. eBird Status and Trends, Data Version: 2022; Released: 2023. https://science.ebird.org/status-and-trends/species/lessca/abundance-map.

Gelman, A. 2006. Prior distributions for variance parameters in hierarchical models (comment on article by Browne and Draper). Bayesian Analysis 1:515–534. https://doi.org/10.1214/06-BA117A.

Gelman, A., J. Carlin B., H. S. Stern, D. Dunson B., A. Vehtari, and D. Rubin B. 2013. *Bayesian Data Analysis*, 3rd edition. Chapman and Hall/CRC. https://doi.org/10.1201/b16018.

Lemoine, N. P. 2019. Moving beyond noninformative priors: why and how to choose weakly informative priors in Bayesian analyses. Oikos 128:912–928. https://doi.org/10.1111/oik.05985.

McElreath, R. 2020. *Statistical Rethinking: A Bayesian Course with Examples in R and STAN*, 2nd edition. Chapman and Hall/CRC, New York. https://doi.org/10.1201/9780429029608.

Supplemental methods for Rufous Hummingbird habitat covariate example

Model structure

The model is an elaboration of the iCAR route-level trend model, where the route-level intercepts and slopes are additive combinations of a component that is a function of a route-level predictor and a residual component, estimated either with the iCAR structure or a non-spatial random effect. The route-level predictors are derived from a habitat modeling study for Rufous Hummingbirds (*Selasphorus rufus*). The mean habitat suitability within a buffer of the BBS route-path is used as a predictor on the intercept (i.e., the mean relative abundance on a given route). The rate of change in habitat suitability over time within the same buffer was used as a predictor on the slope (i.e., the trend in the species' abundance). This model structure relies on relatively simple assumptions that the amount of habitat around a BBS route should predict the number of individual birds, and that the change in the amount of habitat should predict the change in the number of birds.

The original study estimated habitat suitability using spectral remote sensing data and species distribution modelling approaches to detect and quantify habitat loss for the Rufous Hummingbird. Using a combination of Landsat surface reflectance remote sensing imagery and long-term climate data, and observations of Rufous Hummingbird occurrence complied from numerous datasets, the study quantified the annual distribution of habitat suitability over time (1985–2021) across the species' entire breeding range in the Pacific Northwest. The habitat suitability modeling in this study was based on the methods in ((Betts et al. 2022)).

The basic model is the same as all of other models in the main paper.

$$C_{r,j,t} = Negative\ Binomial\left(\lambda_{r,j,t}, \phi\right)$$

$$log\left(\lambda_{r,j,t}\right) = \alpha_r + \beta_r * (t - t_m) + \eta \mathrm{I}j, t + \omega j$$

We modeled the observed counts ($C_{r,j,t}$) of Rufous Hummingbirds on route-r, in year-t, by observer-j as as realizations of a negative binomial distribution, with mean $\lambda_{r,j,t}$ and inverse

dispersion parameter ϕ. The log of the mean ($\lambda_{r,j,t}$) of the negative binomial distribution was modeled as an additive combination of route-level intercepts (α_r), observer-effects (ω_j), and a first-year observer-effect ($\eta I[j,t]$), and route-level slope parameters (β_r) for the continuous effect of year (t) centered on the mid-year of the time-series (t_m).

We estimated the route-level intercepts and slopes as an additive combination of a mean species-level intercept or slope (α' or β'), a varying intercept or slope that was a function of the mean habitat suitability on the route (α_r''') or rate of change in habitat suitability on the slope (β_r'''), and spatially varying effects for the residual variation in relative abundance (α_r'') and slope (β_r'') that were not explained by habitat.

$$\begin{aligned} \alpha_r = &\quad \alpha' + \alpha_r'' + \alpha_r''' \\ \beta_r = &\quad \beta' + \beta_r'' + \beta_r''' \end{aligned}$$

This partitioning of the intercept and slope parameter allows the model to generate two alternative estimates of the mean abundance and trend on each route. The full trend $\beta' + \beta_r'' + \beta_r'''$ represents the full estimated trend on a given route, including the effects of habitat-change. The residual trend $\beta' + \beta_r''$ represents a counter-factual trend that would have been expected if the habitat had stayed constant on a given route. Similarly, the full relative abundance $\alpha' + \alpha_r'' + \alpha_r'''$ represents the full estimated relative abundance on a given route, including the effects of habitat. The residual relative abundance $\alpha' + \alpha_r''$ represents a counter-factual abundance that would have been expected if the habitat suitability was the same across all routes.

We estimated the effect of mean habitat suitability on the route-level intercept as a simple product of a route-specific coefficient (ρ_{α_r}) and the mean (over all years) of the annual habitat suitabilities in a buffer surrounding each route-path ($\alpha_r'' = \rho_{\alpha_r} * \mu_{habitatsuitability_r}$).The annual habitat suitability values are scaled from 0 – 1, so that as scaled, the estimate of ρ_{α_r} represents the maximum possible change in suitability. However, the realized range in values was from 0.2 to 0.7, and so a more relevant interpretation is that it represents twice the maximum change in abundance due to habitat. To model the effects of habitat-change on population trend, we estimated the effect of the rate of change in habitat suitability on each route as a product of a route-specific coefficient (ρ_{β_r}) and an estimate of the average rate of change in habitat suitability on each route ($\delta_{habitatsuitability_r}$). We estimated the rate of change in habitat suitability as the slope of a simple linear regression through the annual estimates of habitat suitability measured within a buffer surrounding each route-path ($\beta_r'' = \rho_{\beta_r} * \delta_{habitatsuitability}$). We multiplied the slopes of the suitability over time by 100, so that they had a standard deviation of approximately 0.5, and so the estimate of ρ_{β_r} represents the change in the log-scale slope parameter associated with the difference between a route on which habitat has been stable and a route where the habitat has increased a lot (i.e., 2 standard deviations from the mean). The habitat suitability predictors were centered to improve convergence. The route-specific coefficients for the effects of habitat suitablility on the intercept and slope were allowed to vary among routes, but were centered on a hyperparameter mean effects across

routes $\rho_{\alpha_r} \sim Normal\left(P_\alpha, \sigma_{\rho_\alpha}\right)$ and $\rho_{\beta_r} \sim Normal\left(P_\beta, \sigma_{\rho_\beta}\right)$. As such, the hyperparameters for the effect of mean habitat suitability on the intercept (P_α) and the effect of change in habitat suitablility on slope (P_β), represent a clear species-level estimate of the overall effects of habitat on abundance and trend, after adjusting for the species mean abundance and trend, as well as the residual spatially dependent variation in abundance and trend.

In the fully spatial implementation of the model, we estimated the residual component of the intercepts and slopes using an intrinsic iCAR structure, where the parameter for route-r is drawn from a normal distribution, centered on the mean of that parameter's values in all neighbouring routes, with an estimated standard deviation that is proportional to the inverse of the number of neighbours for that route (Morris et al. 2019). Specifically, the component of the intercept that represents the residual spatially dependent relative abundance (α_r''') was drawn from a normal distribution centered on the mean of the intercepts for all neighbouring routes.

$$\alpha_r''' \sim Normal\left(\frac{\sum_{n \in N_r} \alpha_n'''}{N_r}, \frac{\sigma_{\alpha'''}}{N_r}\right)$$

The spatially varying component of the slope (${\beta_r}'''$) was estimated similarly as random route-level terms from a normal distribution centered on the mean of the slopes for all neighbouring routes using the same iCAR structure.

$$\beta_r''' \sim Normal\left(\frac{\sum_{n \in N_r} \beta_n'''}{N_r}, \frac{\sigma_{\beta'''}}{N_r}\right)$$

Alternative non-spatial residual term on intercepts

In the fully spatial version of the model, there was a relatively strong spatial autocorrelation in both the habitat suitability and the mean abundance of the species. As a result, the spatial iCAR component of the intercept absorbed much of the variation in abundance among routes, leaving relatively little variation explained by habitat.

Since the spatial component of habitat suitability could reasonably be considered a cause of the spatial dependency in abundance, we drew our final inference on the effect of habitat suitability on abundance from a model that estimated the residual component of the intercept term with a non-spatial varying effect (i.e., a simple random effect). Specifically, the component of the intercept that represents the residual relative abundance (α_r''') was drawn from a normal distribution centered at zero with an estimated standard deviation ($\alpha_r''' \sim Normal(0, \sigma_{\alpha'''})$).

```
library(bbsBayes2)
library(tidyverse)
library(sf)
```

```
library(cmdstanr)
library(patchwork)

output_dir <- "output"
species <- "Rufous Hummingbird"


species_f <- gsub(gsub(species,pattern = " ",replacement = "_",fixed = T)
                  ,pattern = "'",replacement = "",fixed = T)

spp <- "_habitat_"

exp_t <- function(x){
  y <- (exp(x)-1)*100
}

firstYear <- 2006
lastYear <- 2021


out_base <- paste0(species_f,spp,firstYear,"_",lastYear)




sp_data_file <- paste0("data_open/",species_f,"_",firstYear,"_",lastYear,
                       "_covariate_stan_data.RData")


load(sp_data_file)

  mod.file = paste0("models/slope",spp,"route_NB.stan")

stan_data[["fit_spatial"]] <- 0 # this sets an option in the model
# to estimate the residual intercept component using a simple random
# effect, instead of a spatial one. This allows the model to estimate
# variation in abundance that is not predicted by local habitat suitability
# but does not fit an inherently spatial residual structure
# setting this fit_spatial value to 1 uses the iCAR structure to model
# a spatially explicit residual term
```

The `stan_data[["fit_spatial"]] <- 0` line sets a `false` conditional statement in the data

list that allows the model to estimate the residual intercept component using a simple random effect, instead of a spatial one. This allows the model to estimate variation in abundance that is not predicted by local habitat suitability but does not fit an inherently spatial residual structure setting this `stan_data[["fit_spatial"]] <- 1` results in a true conditional statement and uses the iCAR structure to model a spatially explicit residual term on the intercept.

```
slope_model <- cmdstan_model(mod.file, stanc_options = list("Oexperimental"))



stanfit <- slope_model$sample(
  data=stan_data,
  refresh=400,
  iter_sampling=2000,
  iter_warmup=2000,
  parallel_chains = 4)

summ <- stanfit$summary()
print(paste(species, stanfit$time()[["total"]]))

saveRDS(stanfit,
        paste0(output_dir,"/",out_base,"_stanfit.rds"))

saveRDS(summ,
        paste0(output_dir,"/",out_base,"_summ_fit.rds"))

summ %>% arrange(-rhat)
```

Fitting the model

Before fitting the model, we prepared the BBS counts, the neighbourhood structures necessary to estimate the iCAR residual spatial component, and joined them to the habitat suitablity predictors. The full code and data necessary to replicate the data-preparation is available in the online supplement. In brief, we selected all routes on which the species had been observed during and for which we had GIS route-path information that would allow us to estimate the route-specific annual habitat suitability values.

We fit the model using the probablistic programming language Stan (Stan Development Team 2022), accessed through the R-package `cmdstanr` (Gabry and Češnovar 2022). We used a warm-up of 2000 iterations, and `cmdstanr` default settings for other arguments, followed by a draw of 2000 samples from which we estimated the posterior distributions. All parameters in all models converged based on Rhat < 1.02 and bulk effective sample sizes > 500.

Results

During the 15-years from 2006-2021, the species overall population declined steeply. The model estimated an overall change in the population of approximately -43% [-52–33]. Trends were negative across the species' range, but most negative in the coastal regions where the species is also most abundant (Figure 1). The effect of habitat suitability on mean relative abundance was strong and positive ($P_{\alpha} = 3$ [2.2-3.8]), and this effect was robust, whether the residual abundance component was spatially autocorrellated or random. There was a clear positive effect of change in the habitat suitability on trends, such that routes with habitat-loss had more negative population trends $P_{\beta} = 0.025$ [0.0026-0.047]. The greater loss of habitat in the coastal region accounts for most of the increased rates of decline in that region (Figure 2), the residual trend component alone (Figure 2, right panel) does not show the same coastal-decline pattern.

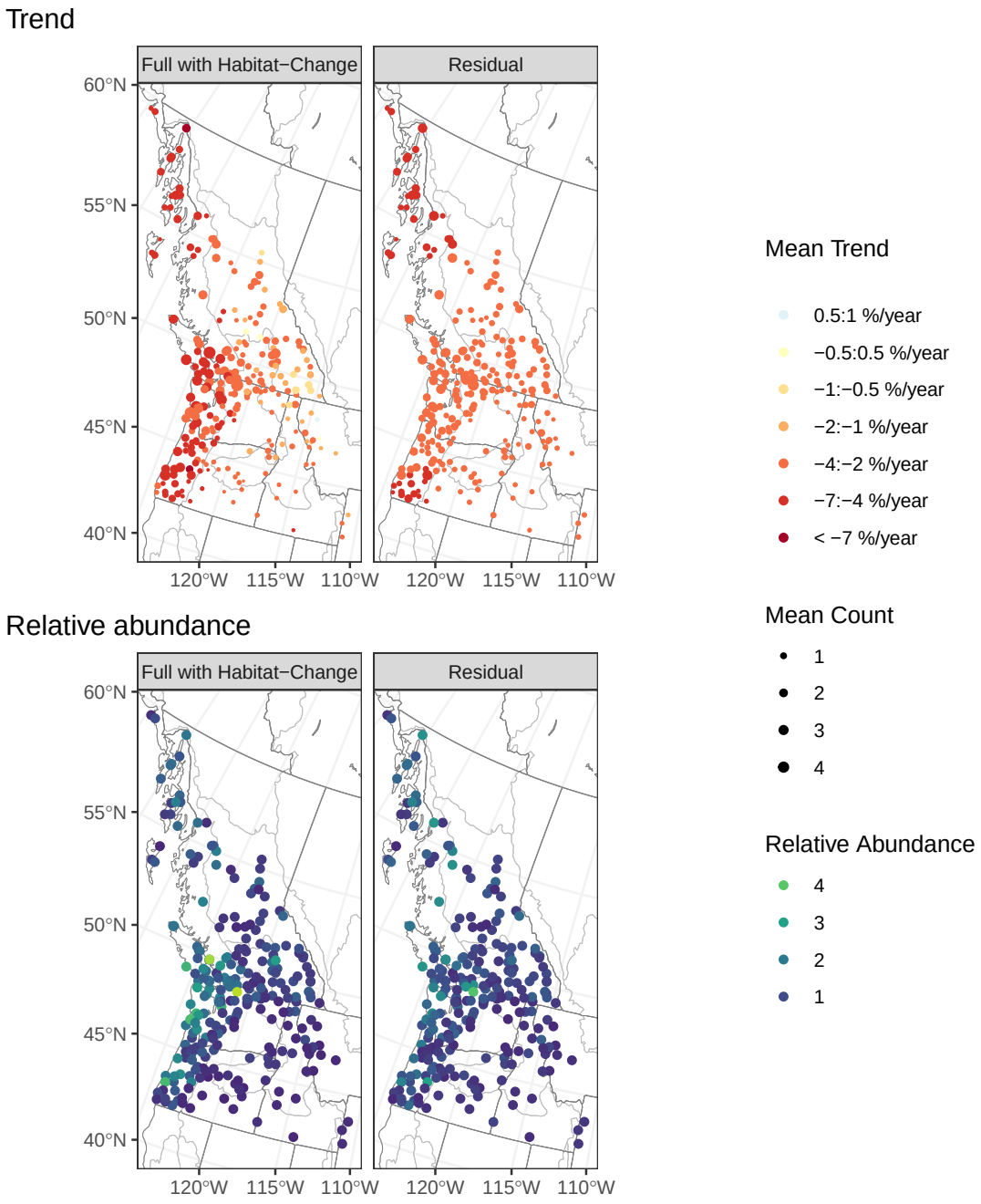

Figure 1: Map of the trends for Rufous Hummingbird from 2006-2021 The colours represent the trends in the uppper panel and the relative abundance in the lower panel. The left panel represents the full estimated trends and abundance on each route, including both the effect of habitat-suitability and the residual component not related to habitat. The right panel represents the trends and relative abundances after removing the effect of habitat-suitability. In the top-left panel, the greater declines in coastal regions are evident from the darker red points compared to the top-right panel. In the bottom-left panel, the higher abundance near the coast is evident from the lighter colours. The bottom-right panel shows much more even relative abundance across the species' range, showing that habitat suitability accounts for much of the variation in abundance

References

Betts, Matthew G., Zhiqiang Yang, Adam S. Hadley, Adam C. Smith, Josée S. Rousseau, Joseph M. Northrup, Joseph J. Nocera, Noel Gorelick, and Brian D. Gerber. 2022. "Forest Degradation Drives Widespread Avian Habitat and Population Declines." *Nature Ecology & Evolution* 6 (6): 709–19. https://doi.org/10.1038/s41559-022-01737-8.

Gabry, Jonah, and Rok Cešnovar. 2022. *Cmdstanr: R Interface to 'CmdStan'*. https://mc-stan.org/cmdstanr.

Morris, Mitzi, Katherine Wheeler-Martin, Dan Simpson, Stephen J. Mooney, Andrew Gelman, and Charles DiMaggio. 2019. "Bayesian Hierarchical Spatial Models: Implementing the Besag York Mollié Model in Stan." *Spatial and Spatio-Temporal Epidemiology* 31 (November): 100301. https://doi.org/10.1016/j.sste.2019.100301.

Stan Development Team, 2.29. 2022. *Stan Modeling Language Users Guide and Reference Manual*. https://mc-stan.org.

Supplemental methods for Horned Grebe habitat covariate example

Model structure

The model is an elaboration of the iCAR route-level trend model, where the route-level intercepts and slopes are estimates of relative abundances and trends, after accounting for the effects of annual fluctuations caused by a route-level annual climate-related predictor. The route-level predictors are derived from a study of the effects of moisture/drought patterns on Horned Grebe (*Podiceps auritus*) trends in Canada. To represent annual variation in available habitat for wetland birds, we used the data collected by the United States Fish and Wildlife Service and the Canadian Wildlife Service on the number of ponds (primarily, temporary small wetlands often referred to as "Prairie Potholes") during aerial surveys (Waterfowl Breeding Population and Habitat Survey Data. 1955-2022)[https://ecos.fws.gov/ServCat/Reference/Profile/140698]. Annual fluctuations in moisture have a strong influence on the number of these wetlands available for waterbird habitat in the Prairie Pothole region of Canada. These annual fluctuations could complicate assessments of a possible long-term decline in the species' population, if strong short-term fluctuations in the amount of habitat being surveyed could overwhelm or counter-act longer-term gradual changes in populations. We designed this model to estimate the long-term rate of population change after statistically controlling for the annual variations in available habitat.

The model is based on the iCAR models in the main paper, but includes count-level predictors for the effects of available habitat.

$$C_{r,j,t} = Negative\ Binomial\left(\lambda_{r,j,t}, \phi\right)$$

$$log\left(\lambda_{r,j,t}\right) = \alpha_r + \beta_r * (t - t_m) + \rho_r * ponds_{r,t} + \eta \mathrm{I} j, t + \omega j$$

We modeled the observed counts ($C_{r,j,t}$) of Horned Grebes on route-r, in year-t, by observer-j as as realizations of a negative binomial distribution, with mean $\lambda_{r,j,t}$ and inverse dispersion

parameter ϕ. The log of the mean ($\lambda_{r,j,t}$) of the negative binomial distribution was modeled as an additive combination of route-level intercepts (α_r), observer-effects (ω_j), and a first-year observer-effect ($\eta I[j,t]$), and route-level slope parameters (β_r) for the continuous effect of year (t) centered on the mid-year of the time-series (t_m).

We estimated the effect of the number of ponds surrounding each route in a given year on BBS counts as a spatially-varying coefficient representing the route-specific effect of local ponds ($\rho_r * ponds_{r,t}$). Where $ponds_{r,t}$ represents the log(1 + number of ponds) surrounding BBS route r in year t, centered on their mean across years for each route. This route-specific centering ensured we could separately estimate the route-level intercepts and the effects of the annual variations in ponds. The effects of ponds at each route were centered on a mean hyperparameter P, and allowed to vary among routes using the same iCAR spatial structure as for the slopes and intercepts (ρ'_r.

$$\rho_r = P + \rho'_r$$
$$\rho'_r \sim Normal\left(\frac{\sum_{n \in N_r} \rho'_n}{N_r}, \frac{\sigma_{\rho'}}{N_r}\right)$$

Finally, we also fit the same data to the simple iCAR model (i.e., an identical model with no covariates) to compare the difference in estimated trends with and without accounting for the annual variations in available habitat.

Fitting the model

To fit the model, we prepared the BBS counts, the neighbourhood structures necessary to estimate the iCAR trend and covariate spatial components, and joined the climate predictor to the data. The full code and data necessary to replicate the data-preparation is available in the online supplement. In brief, we selected all routes on which the species had been observed in the years 1975 - 2017, and for which we had ponds data (Prairie-pothole region of Canada).

We fit the model using the probabilistic programming language Stan (Stan Development Team 2022), accessed through the R-package `cmdstanr` (Gabry and Češnovar 2022). We used a warm-up of 2000 iterations, and `cmdstanr` default settings for other arguments, followed by a draw of 2000 samples from which we estimated the posterior distributions. All parameters in all models converged based on Rhat < 1.02 and bulk effective sample sizes > 500 (Gelman et al. 2020).

Results

During the 43-years from 1975-2017, the species population declined at a rate of -1.9 %/year. After removing the effect of annual variations in the number of ponds surrounding each BBS route, the long-term rate of decline was -2.2 %/year. This difference suggests that annual fluctuations in moisture, such as the relatively high-moisture periods in 2014-2017, have been responsible for reducing the species' rate of decline. It also suggests that the species' Prairie populations may decline even further in the future, given the predictions for reduced precipitation and higher temperatures in the region with ongoing climate change.

The effect of annual fluctuations in the number of ponds was positive across the region: the mean value of $P = 0.42$ $[0.29 : 0.55]$. but there was also a spatial gradient in intensity. The effect of number of ponds in a given year was strongest in the western part of the Prairies (Figure 1). This spatial pattern makes sense given that the western prairies tend to experience more intense and frequent drought conditions ((Millett, Johnson, and Guntenspergen 2009)).

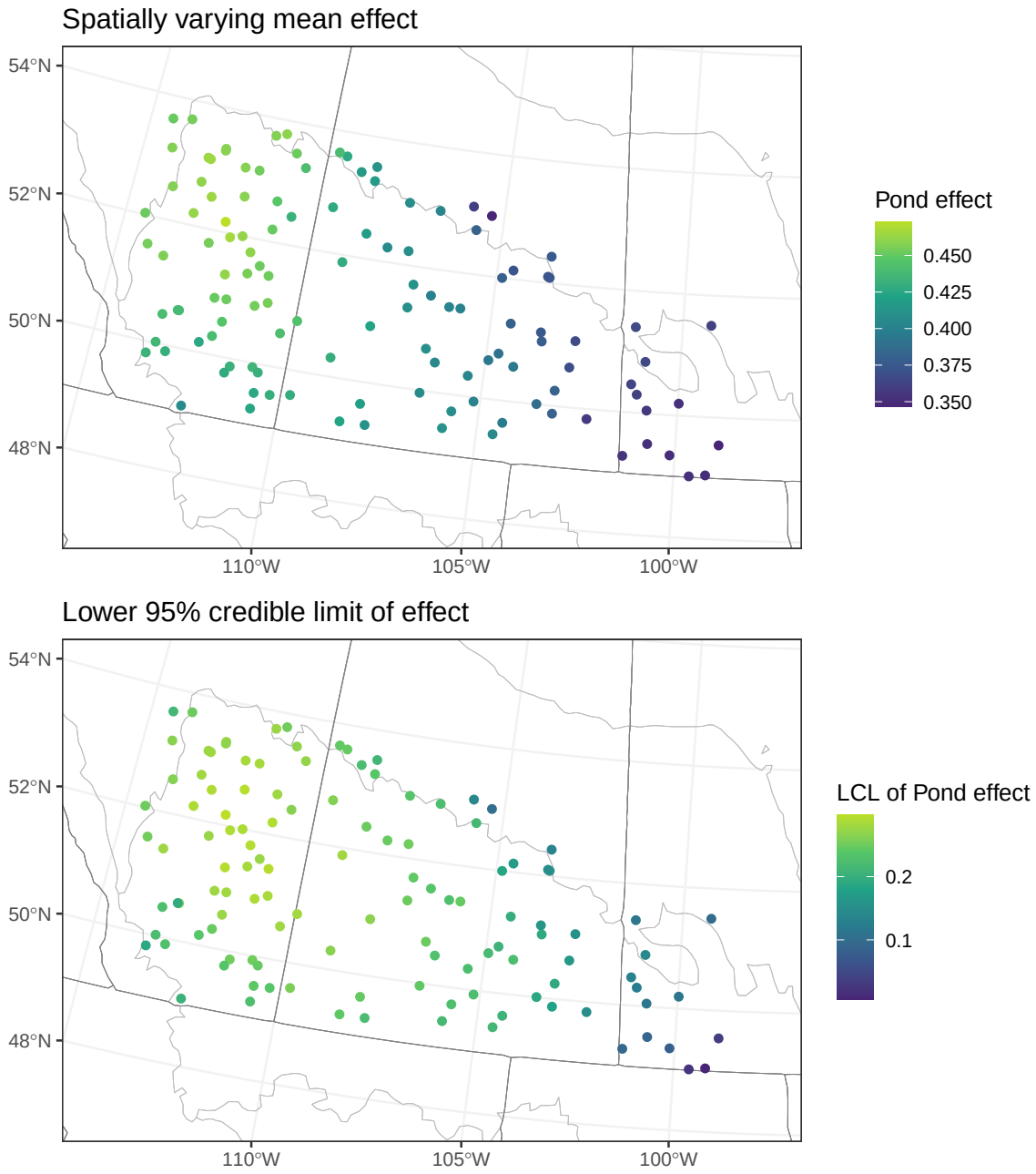

Figure 1: Map of the effect of the number of ponds surrounding each BBS route in a given year on the counts of Horned Grebes, 1975-2017. The colours represent the route-specific coefficient for the effect of the log-transformed count of the number of ponds surrounding each Breeding Bird Survey route. The more positive values (lighter colours) indicate a stronger positive effect of the number of ponds (available habitat) during a given year on counts of Horned Grebes during a given survey. The upper panel shows the posterior mean effects at each route and the lower panel shows the lower 95% credible limit for the effect.

References

Gabry, Jonah, and Rok Cešnovar. 2022. *Cmdstanr: R Interface to 'CmdStan'*. https://mc-stan.org/cmdstanr.

Gelman, Andrew, Aki Vehtari, Daniel Simpson, Charles C. Margossian, Bob Carpenter, Yuling Yao, Lauren Kennedy, Jonah Gabry, Paul-Christian Bürkner, and Martin Modrák. 2020. "Bayesian Workflow." *arXiv:2011.01808 [Stat]*, November. http://arxiv.org/abs/2011.01808.

Millett, Bruce, W. Carter Johnson, and Glenn Guntenspergen. 2009. "Climate Trends of the North American Prairie Pothole Region 1906–2000." *Climatic Change* 93 (1): 243–67. https://doi.org/10.1007/s10584-008-9543-5.

Stan Development Team, 2.29. 2022. *Stan Modeling Language Users Guide and Reference Manual*. https://mc-stan.org.

Table S1. The list of species names for the 287 species included in this study and which of the four models we fit to each species. Species sorted by taxonomic order.

English common name	Latin species name	Models fit
Black-bellied Whistling-Duck	*Dendrocygna autumnalis*	Non-spatial, iCAR, BYM, and GP
Canada Goose	*Branta canadensis*	Non-spatial, iCAR
Wood Duck	*Aix sponsa*	Non-spatial, iCAR
Blue-winged Teal	*Spatula discors*	Non-spatial, iCAR
Northern Shoveler	*Spatula clypeata*	Non-spatial, iCAR
Gadwall	*Mareca strepera*	Non-spatial, iCAR
American Wigeon	*Mareca americana*	Non-spatial, iCAR
Mallard	*Anas platyrhynchos*	Non-spatial, iCAR
Northern Pintail	*Anas acuta*	Non-spatial, iCAR
Green-winged Teal	*Anas crecca*	Non-spatial, iCAR
Ring-necked Duck	*Aythya collaris*	Non-spatial, iCAR
Lesser Scaup	*Aythya affinis*	Non-spatial, iCAR, BYM, and GP
Common Merganser	*Mergus merganser*	Non-spatial, iCAR
Mountain Quail	*Oreortyx pictus*	Non-spatial, iCAR, BYM, and GP
Northern Bobwhite	*Colinus virginianus*	Non-spatial, iCAR
Scaled Quail	*Callipepla squamata*	Non-spatial, iCAR, BYM, and GP
California Quail	*Callipepla californica*	Non-spatial, iCAR, BYM, and GP
Wild Turkey	*Meleagris gallopavo*	Non-spatial, iCAR
Ruffed Grouse	*Bonasa umbellus*	Non-spatial, iCAR
Ring-necked Pheasant	*Phasianus colchicus*	Non-spatial, iCAR
Pied-billed Grebe	*Podilymbus podiceps*	Non-spatial, iCAR
Rock Pigeon	*Columba livia*	Non-spatial, iCAR
Band-tailed Pigeon	*Patagioenas fasciata*	Non-spatial, iCAR, BYM, and GP
Eurasian Collared-Dove	*Streptopelia decaocto*	Non-spatial, iCAR
Inca Dove	*Columbina inca*	Non-spatial, iCAR, BYM, and GP
Common Ground Dove	*Columbina passerina*	Non-spatial, iCAR, BYM, and GP
White-winged Dove	*Zenaida asiatica*	Non-spatial, iCAR, BYM, and GP
Mourning Dove	*Zenaida macroura*	Non-spatial, iCAR
Greater Roadrunner	*Geococcyx californianus*	Non-spatial, iCAR, BYM, and GP
Yellow-billed Cuckoo	*Coccyzus americanus*	Non-spatial, iCAR
Black-billed Cuckoo	*Coccyzus erythropthalmus*	Non-spatial, iCAR
Lesser Nighthawk	*Chordeiles acutipennis*	Non-spatial, iCAR, BYM, and GP
Common Nighthawk	*Chordeiles minor*	Non-spatial, iCAR
Chuck-will's-widow	*Antrostomus carolinensis*	Non-spatial, iCAR
Chimney Swift	*Chaetura pelagica*	Non-spatial, iCAR
Ruby-throated Hummingbird	*Archilochus colubris*	Non-spatial, iCAR
Anna's Hummingbird	*Calypte anna*	Non-spatial, iCAR, BYM, and GP
Rufous Hummingbird	*Selasphorus rufus*	Non-spatial, iCAR, BYM, and GP
Broad-tailed Hummingbird	*Selasphorus platycercus*	Non-spatial, iCAR, BYM, and GP
Sora	*Porzana carolina*	Non-spatial, iCAR
American Coot	*Fulica americana*	Non-spatial, iCAR
Sandhill Crane	*Antigone canadensis*	Non-spatial, iCAR
Killdeer	*Charadrius vociferus*	Non-spatial, iCAR

Table S1. The list of species names for the 287 species included in this study and which of the four models we fit to each species. Species sorted by taxonomic order.

English common name	Latin species name	Models fit
Upland Sandpiper	*Bartramia longicauda*	Non-spatial, iCAR
Long-billed Curlew	*Numenius americanus*	Non-spatial, iCAR, BYM, and GP
Marbled Godwit	*Limosa fedoa*	Non-spatial, iCAR, BYM, and GP
Wilson's Snipe	*Gallinago delicata*	Non-spatial, iCAR
Spotted Sandpiper	*Actitis macularius*	Non-spatial, iCAR
Willet	*Tringa semipalmata*	Non-spatial, iCAR
Wilson's Phalarope	*Phalaropus tricolor*	Non-spatial, iCAR
Laughing Gull	*Leucophaeus atricilla*	Non-spatial, iCAR, BYM, and GP
Ring-billed Gull	*Larus delawarensis*	Non-spatial, iCAR
Herring Gull	*Larus argentatus*	Non-spatial, iCAR
Common Loon	*Gavia immer*	Non-spatial, iCAR
Double-crested Cormorant	*Nannopterum auritum*	Non-spatial, iCAR
American White Pelican	*Pelecanus erythrorhynchos*	Non-spatial, iCAR
American Bittern	*Botaurus lentiginosus*	Non-spatial, iCAR
Great Blue Heron	*Ardea herodias*	Non-spatial, iCAR
Great Egret	*Ardea alba*	Non-spatial, iCAR
Little Blue Heron	*Egretta caerulea*	Non-spatial, iCAR
Cattle Egret	*Bubulcus ibis*	Non-spatial, iCAR
Green Heron	*Butorides virescens*	Non-spatial, iCAR
White Ibis	*Eudocimus albus*	Non-spatial, iCAR, BYM, and GP
Black Vulture	*Coragyps atratus*	Non-spatial, iCAR
Turkey Vulture	*Cathartes aura*	Non-spatial, iCAR
Osprey	*Pandion haliaetus*	Non-spatial, iCAR
Golden Eagle	*Aquila chrysaetos*	Non-spatial, iCAR
Northern Harrier	*Circus hudsonius*	Non-spatial, iCAR
Sharp-shinned Hawk	*Accipiter striatus*	Non-spatial, iCAR
Cooper's Hawk	*Accipiter cooperii*	Non-spatial, iCAR
Bald Eagle	*Haliaeetus leucocephalus*	Non-spatial, iCAR
Mississippi Kite	*Ictinia mississippiensis*	Non-spatial, iCAR
Red-shouldered Hawk	*Buteo lineatus*	Non-spatial, iCAR
Broad-winged Hawk	*Buteo platypterus*	Non-spatial, iCAR
Swainson's Hawk	*Buteo swainsoni*	Non-spatial, iCAR
Great Horned Owl	*Bubo virginianus*	Non-spatial, iCAR
Barred Owl	*Strix varia*	Non-spatial, iCAR
Belted Kingfisher	*Megaceryle alcyon*	Non-spatial, iCAR
Red-headed Woodpecker	*Melanerpes erythrocephalus*	Non-spatial, iCAR
Acorn Woodpecker	*Melanerpes formicivorus*	Non-spatial, iCAR, BYM, and GP
Red-bellied Woodpecker	*Melanerpes carolinus*	Non-spatial, iCAR
Yellow-bellied Sapsucker	*Sphyrapicus varius*	Non-spatial, iCAR
Red-naped Sapsucker	*Sphyrapicus nuchalis*	Non-spatial, iCAR, BYM, and GP
Red-breasted Sapsucker	*Sphyrapicus ruber*	Non-spatial, iCAR, BYM, and GP
Downy Woodpecker	*Dryobates pubescens*	Non-spatial, iCAR
Ladder-backed Woodpecker	*Dryobates scalaris*	Non-spatial, iCAR, BYM, and GP

Table S1. The list of species names for the 287 species included in this study and which of the four models we fit to each species. Species sorted by taxonomic order.

English common name	Latin species name	Models fit
Hairy Woodpecker	*Dryobates villosus*	Non-spatial, iCAR
Pileated Woodpecker	*Dryocopus pileatus*	Non-spatial, iCAR
Crested Caracara	*Caracara plancus*	Non-spatial, iCAR, BYM, and GP
American Kestrel	*Falco sparverius*	Non-spatial, iCAR
Merlin	*Falco columbarius*	Non-spatial, iCAR
Ash-throated Flycatcher	*Myiarchus cinerascens*	Non-spatial, iCAR
Great Crested Flycatcher	*Myiarchus crinitus*	Non-spatial, iCAR
Cassin's Kingbird	*Tyrannus vociferans*	Non-spatial, iCAR, BYM, and GP
Western Kingbird	*Tyrannus verticalis*	Non-spatial, iCAR
Eastern Kingbird	*Tyrannus tyrannus*	Non-spatial, iCAR
Scissor-tailed Flycatcher	*Tyrannus forficatus*	Non-spatial, iCAR
Olive-sided Flycatcher	*Contopus cooperi*	Non-spatial, iCAR
Western Wood-Pewee	*Contopus sordidulus*	Non-spatial, iCAR
Eastern Wood-Pewee	*Contopus virens*	Non-spatial, iCAR
Yellow-bellied Flycatcher	*Empidonax flaviventris*	Non-spatial, iCAR
Acadian Flycatcher	*Empidonax virescens*	Non-spatial, iCAR
Alder Flycatcher	*Empidonax alnorum*	Non-spatial, iCAR
Willow Flycatcher	*Empidonax traillii*	Non-spatial, iCAR
Least Flycatcher	*Empidonax minimus*	Non-spatial, iCAR
Hammond's Flycatcher	*Empidonax hammondii*	Non-spatial, iCAR
Gray Flycatcher	*Empidonax wrightii*	Non-spatial, iCAR, BYM, and GP
Dusky Flycatcher	*Empidonax oberholseri*	Non-spatial, iCAR
Pacific-slope Flycatcher	*Empidonax difficilis*	Non-spatial, iCAR, BYM, and GP
Cordilleran Flycatcher	*Empidonax occidentalis*	Non-spatial, iCAR, BYM, and GP
Black Phoebe	*Sayornis nigricans*	Non-spatial, iCAR, BYM, and GP
Eastern Phoebe	*Sayornis phoebe*	Non-spatial, iCAR
Say's Phoebe	*Sayornis saya*	Non-spatial, iCAR
White-eyed Vireo	*Vireo griseus*	Non-spatial, iCAR
Bell's Vireo	*Vireo bellii*	Non-spatial, iCAR
Hutton's Vireo	*Vireo huttoni*	Non-spatial, iCAR, BYM, and GP
Yellow-throated Vireo	*Vireo flavifrons*	Non-spatial, iCAR
Cassin's Vireo	*Vireo cassinii*	Non-spatial, iCAR, BYM, and GP
Blue-headed Vireo	*Vireo solitarius*	Non-spatial, iCAR
Plumbeous Vireo	*Vireo plumbeus*	Non-spatial, iCAR, BYM, and GP
Warbling Vireo	*Vireo gilvus*	Non-spatial, iCAR
Red-eyed Vireo	*Vireo olivaceus*	Non-spatial, iCAR
Loggerhead Shrike	*Lanius ludovicianus*	Non-spatial, iCAR
Canada Jay	*Perisoreus canadensis*	Non-spatial, iCAR
Pinyon Jay	*Gymnorhinus cyanocephalus*	Non-spatial, iCAR, BYM, and GP
Steller's Jay	*Cyanocitta stelleri*	Non-spatial, iCAR
Blue Jay	*Cyanocitta cristata*	Non-spatial, iCAR
California Scrub-Jay	*Aphelocoma californica*	Non-spatial, iCAR, BYM, and GP
Woodhouse's Scrub-Jay	*Aphelocoma woodhouseii*	Non-spatial, iCAR, BYM, and GP

Table S1. The list of species names for the 287 species included in this study and which of the four models we fit to each species. Species sorted by taxonomic order.

English common name	Latin species name	Models fit
Clark's Nutcracker	*Nucifraga columbiana*	Non-spatial, iCAR, BYM, and GP
Black-billed Magpie	*Pica hudsonia*	Non-spatial, iCAR
American Crow	*Corvus brachyrhynchos*	Non-spatial, iCAR
Fish Crow	*Corvus ossifragus*	Non-spatial, iCAR
Chihuahuan Raven	*Corvus cryptoleucus*	Non-spatial, iCAR, BYM, and GP
Common Raven	*Corvus corax*	Non-spatial, iCAR
Verdin	*Auriparus flaviceps*	Non-spatial, iCAR, BYM, and GP
Carolina Chickadee	*Poecile carolinensis*	Non-spatial, iCAR
Black-capped Chickadee	*Poecile atricapillus*	Non-spatial, iCAR
Mountain Chickadee	*Poecile gambeli*	Non-spatial, iCAR
Chestnut-backed Chickadee	*Poecile rufescens*	Non-spatial, iCAR, BYM, and GP
Boreal Chickadee	*Poecile hudsonicus*	Non-spatial, iCAR
Juniper Titmouse	*Baeolophus ridgwayi*	Non-spatial, iCAR, BYM, and GP
Tufted Titmouse	*Baeolophus bicolor*	Non-spatial, iCAR
Horned Lark	*Eremophila alpestris*	Non-spatial, iCAR
Bank Swallow	*Riparia riparia*	Non-spatial, iCAR
Tree Swallow	*Tachycineta bicolor*	Non-spatial, iCAR
Violet-green Swallow	*Tachycineta thalassina*	Non-spatial, iCAR
Northern Rough-winged Swallow	*Stelgidopteryx serripennis*	Non-spatial, iCAR
Purple Martin	*Progne subis*	Non-spatial, iCAR
Barn Swallow	*Hirundo rustica*	Non-spatial, iCAR
Cliff Swallow	*Petrochelidon pyrrhonota*	Non-spatial, iCAR
Cave Swallow	*Petrochelidon fulva*	Non-spatial, iCAR, BYM, and GP
Bushtit	*Psaltriparus minimus*	Non-spatial, iCAR, BYM, and GP
Wrentit	*Chamaea fasciata*	Non-spatial, iCAR, BYM, and GP
Ruby-crowned Kinglet	*Corthylio calendula*	Non-spatial, iCAR
Golden-crowned Kinglet	*Regulus satrapa*	Non-spatial, iCAR
Cedar Waxwing	*Bombycilla cedrorum*	Non-spatial, iCAR
Phainopepla	*Phainopepla nitens*	Non-spatial, iCAR, BYM, and GP
Red-breasted Nuthatch	*Sitta canadensis*	Non-spatial, iCAR
White-breasted Nuthatch	*Sitta carolinensis*	Non-spatial, iCAR
Pygmy Nuthatch	*Sitta pygmaea*	Non-spatial, iCAR, BYM, and GP
Brown-headed Nuthatch	*Sitta pusilla*	Non-spatial, iCAR
Brown Creeper	*Certhia americana*	Non-spatial, iCAR
Blue-gray Gnatcatcher	*Polioptila caerulea*	Non-spatial, iCAR
Rock Wren	*Salpinctes obsoletus*	Non-spatial, iCAR
Cactus Wren	*Campylorhynchus brunneicapillus*	Non-spatial, iCAR, BYM, and GP
Bewick's Wren	*Thryomanes bewickii*	Non-spatial, iCAR
Carolina Wren	*Thryothorus ludovicianus*	Non-spatial, iCAR
House Wren	*Troglodytes aedon*	Non-spatial, iCAR
Pacific Wren	*Troglodytes pacificus*	Non-spatial, iCAR, BYM, and GP
Winter Wren	*Troglodytes hiemalis*	Non-spatial, iCAR
Sedge Wren	*Cistothorus stellaris*	Non-spatial, iCAR

Table S1. The list of species names for the 287 species included in this study and which of the four models we fit to each species. Species sorted by taxonomic order.

English common name	Latin species name	Models fit
Marsh Wren	*Cistothorus palustris*	Non-spatial, iCAR
Gray Catbird	*Dumetella carolinensis*	Non-spatial, iCAR
Curve-billed Thrasher	*Toxostoma curvirostre*	Non-spatial, iCAR, BYM, and GP
Brown Thrasher	*Toxostoma rufum*	Non-spatial, iCAR
Sage Thrasher	*Oreoscoptes montanus*	Non-spatial, iCAR, BYM, and GP
Northern Mockingbird	*Mimus polyglottos*	Non-spatial, iCAR
European Starling	*Sturnus vulgaris*	Non-spatial, iCAR
Eastern Bluebird	*Sialia sialis*	Non-spatial, iCAR
Western Bluebird	*Sialia mexicana*	Non-spatial, iCAR, BYM, and GP
Mountain Bluebird	*Sialia currucoides*	Non-spatial, iCAR
Townsend's Solitaire	*Myadestes townsendi*	Non-spatial, iCAR
Veery	*Catharus fuscescens*	Non-spatial, iCAR
Swainson's Thrush	*Catharus ustulatus*	Non-spatial, iCAR
Hermit Thrush	*Catharus guttatus*	Non-spatial, iCAR
Wood Thrush	*Hylocichla mustelina*	Non-spatial, iCAR
American Robin	*Turdus migratorius*	Non-spatial, iCAR
Varied Thrush	*Ixoreus naevius*	Non-spatial, iCAR, BYM, and GP
House Sparrow	*Passer domesticus*	Non-spatial, iCAR
Sprague's Pipit	*Anthus spragueii*	Non-spatial, iCAR, BYM, and GP
Evening Grosbeak	*Coccothraustes vespertinus*	Non-spatial, iCAR
House Finch	*Haemorhous mexicanus*	Non-spatial, iCAR
Purple Finch	*Haemorhous purpureus*	Non-spatial, iCAR
Cassin's Finch	*Haemorhous cassinii*	Non-spatial, iCAR, BYM, and GP
Common Redpoll	*Acanthis flammea*	Non-spatial, iCAR, BYM, and GP
Red Crossbill	*Loxia curvirostra*	Non-spatial, iCAR
White-winged Crossbill	*Loxia leucoptera*	Non-spatial, iCAR
Pine Siskin	*Spinus pinus*	Non-spatial, iCAR
Lesser Goldfinch	*Spinus psaltria*	Non-spatial, iCAR
American Goldfinch	*Spinus tristis*	Non-spatial, iCAR
Chestnut-collared Longspur	*Calcarius ornatus*	Non-spatial, iCAR, BYM, and GP
Cassin's Sparrow	*Peucaea cassinii*	Non-spatial, iCAR, BYM, and GP
Grasshopper Sparrow	*Ammodramus savannarum*	Non-spatial, iCAR
Black-throated Sparrow	*Amphispiza bilineata*	Non-spatial, iCAR, BYM, and GP
Lark Sparrow	*Chondestes grammacus*	Non-spatial, iCAR
Lark Bunting	*Calamospiza melanocorys*	Non-spatial, iCAR, BYM, and GP
Chipping Sparrow	*Spizella passerina*	Non-spatial, iCAR
Clay-colored Sparrow	*Spizella pallida*	Non-spatial, iCAR
Field Sparrow	*Spizella pusilla*	Non-spatial, iCAR
Brewer's Sparrow	*Spizella breweri*	Non-spatial, iCAR
Fox Sparrow	*Passerella iliaca*	Non-spatial, iCAR
White-crowned Sparrow	*Zonotrichia leucophrys*	Non-spatial, iCAR
White-throated Sparrow	*Zonotrichia albicollis*	Non-spatial, iCAR
Sagebrush Sparrow	*Artemisiospiza nevadensis*	Non-spatial, iCAR, BYM, and GP

Table S1. The list of species names for the 287 species included in this study and which of the four models we fit to each species. Species sorted by taxonomic order.

English common name	Latin species name	Models fit
Vesper Sparrow	*Pooecetes gramineus*	Non-spatial, iCAR
LeConte's Sparrow	*Ammospiza leconteii*	Non-spatial, iCAR, BYM, and GP
Baird's Sparrow	*Centronyx bairdii*	Non-spatial, iCAR, BYM, and GP
Savannah Sparrow	*Passerculus sandwichensis*	Non-spatial, iCAR
Song Sparrow	*Melospiza melodia*	Non-spatial, iCAR
Lincoln's Sparrow	*Melospiza lincolnii*	Non-spatial, iCAR
Swamp Sparrow	*Melospiza georgiana*	Non-spatial, iCAR
Canyon Towhee	*Melozone fusca*	Non-spatial, iCAR, BYM, and GP
Rufous-crowned Sparrow	*Aimophila ruficeps*	Non-spatial, iCAR, BYM, and GP
Green-tailed Towhee	*Pipilo chlorurus*	Non-spatial, iCAR, BYM, and GP
Spotted Towhee	*Pipilo maculatus*	Non-spatial, iCAR
Eastern Towhee	*Pipilo erythrophthalmus*	Non-spatial, iCAR
Yellow-breasted Chat	*Icteria virens*	Non-spatial, iCAR
Yellow-headed Blackbird	*Xanthocephalus xanthocephalus*	Non-spatial, iCAR
Bobolink	*Dolichonyx oryzivorus*	Non-spatial, iCAR
Eastern Meadowlark	*Sturnella magna*	Non-spatial, iCAR
Western Meadowlark	*Sturnella neglecta*	Non-spatial, iCAR
Orchard Oriole	*Icterus spurius*	Non-spatial, iCAR
Bullock's Oriole	*Icterus bullockii*	Non-spatial, iCAR
Baltimore Oriole	*Icterus galbula*	Non-spatial, iCAR
Scott's Oriole	*Icterus parisorum*	Non-spatial, iCAR, BYM, and GP
Red-winged Blackbird	*Agelaius phoeniceus*	Non-spatial, iCAR
Brown-headed Cowbird	*Molothrus ater*	Non-spatial, iCAR
Brewer's Blackbird	*Euphagus cyanocephalus*	Non-spatial, iCAR
Common Grackle	*Quiscalus quiscula*	Non-spatial, iCAR
Boat-tailed Grackle	*Quiscalus major*	Non-spatial, iCAR, BYM, and GP
Great-tailed Grackle	*Quiscalus mexicanus*	Non-spatial, iCAR
Ovenbird	*Seiurus aurocapilla*	Non-spatial, iCAR
Worm-eating Warbler	*Helmitheros vermivorum*	Non-spatial, iCAR
Louisiana Waterthrush	*Parkesia motacilla*	Non-spatial, iCAR
Northern Waterthrush	*Parkesia noveboracensis*	Non-spatial, iCAR
Golden-winged Warbler	*Vermivora chrysoptera*	Non-spatial, iCAR, BYM, and GP
Blue-winged Warbler	*Vermivora cyanoptera*	Non-spatial, iCAR
Black-and-white Warbler	*Mniotilta varia*	Non-spatial, iCAR
Prothonotary Warbler	*Protonotaria citrea*	Non-spatial, iCAR
Tennessee Warbler	*Leiothlypis peregrina*	Non-spatial, iCAR
Orange-crowned Warbler	*Leiothlypis celata*	Non-spatial, iCAR
Nashville Warbler	*Leiothlypis ruficapilla*	Non-spatial, iCAR
MacGillivray's Warbler	*Geothlypis tolmiei*	Non-spatial, iCAR
Mourning Warbler	*Geothlypis philadelphia*	Non-spatial, iCAR
Kentucky Warbler	*Geothlypis formosa*	Non-spatial, iCAR
Common Yellowthroat	*Geothlypis trichas*	Non-spatial, iCAR
Hooded Warbler	*Setophaga citrina*	Non-spatial, iCAR

Table S1. The list of species names for the 287 species included in this study and which of the four models we fit to each species. Species sorted by taxonomic order.

English common name	Latin species name	Models fit
American Redstart	*Setophaga ruticilla*	Non-spatial, iCAR
Cerulean Warbler	*Setophaga cerulea*	Non-spatial, iCAR, BYM, and GP
Northern Parula	*Setophaga americana*	Non-spatial, iCAR
Magnolia Warbler	*Setophaga magnolia*	Non-spatial, iCAR
Blackburnian Warbler	*Setophaga fusca*	Non-spatial, iCAR
Yellow Warbler	*Setophaga petechia*	Non-spatial, iCAR
Chestnut-sided Warbler	*Setophaga pensylvanica*	Non-spatial, iCAR
Blackpoll Warbler	*Setophaga striata*	Non-spatial, iCAR, BYM, and GP
Black-throated Blue Warbler	*Setophaga caerulescens*	Non-spatial, iCAR
Pine Warbler	*Setophaga pinus*	Non-spatial, iCAR
Yellow-throated Warbler	*Setophaga dominica*	Non-spatial, iCAR
Prairie Warbler	*Setophaga discolor*	Non-spatial, iCAR
Black-throated Gray Warbler	*Setophaga nigrescens*	Non-spatial, iCAR, BYM, and GP
Townsend's Warbler	*Setophaga townsendi*	Non-spatial, iCAR, BYM, and GP
Hermit Warbler	*Setophaga occidentalis*	Non-spatial, iCAR, BYM, and GP
Black-throated Green Warbler	*Setophaga virens*	Non-spatial, iCAR
Canada Warbler	*Cardellina canadensis*	Non-spatial, iCAR
Wilson's Warbler	*Cardellina pusilla*	Non-spatial, iCAR
Summer Tanager	*Piranga rubra*	Non-spatial, iCAR
Scarlet Tanager	*Piranga olivacea*	Non-spatial, iCAR
Western Tanager	*Piranga ludoviciana*	Non-spatial, iCAR
Northern Cardinal	*Cardinalis cardinalis*	Non-spatial, iCAR
Rose-breasted Grosbeak	*Pheucticus ludovicianus*	Non-spatial, iCAR
Black-headed Grosbeak	*Pheucticus melanocephalus*	Non-spatial, iCAR
Blue Grosbeak	*Passerina caerulea*	Non-spatial, iCAR
Lazuli Bunting	*Passerina amoena*	Non-spatial, iCAR
Indigo Bunting	*Passerina cyanea*	Non-spatial, iCAR
Painted Bunting	*Passerina ciris*	Non-spatial, iCAR
Dickcissel	*Spiza americana*	Non-spatial, iCAR

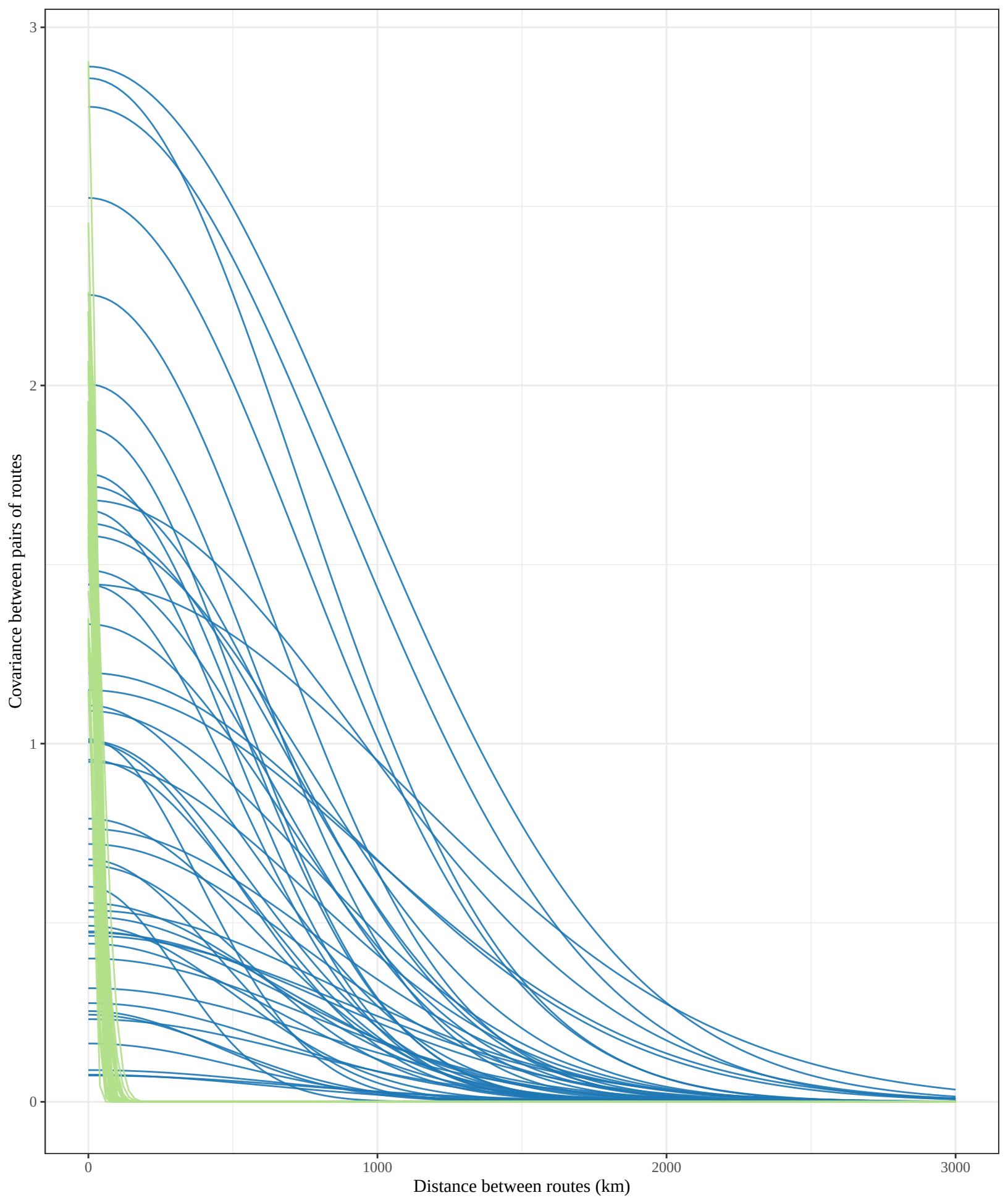

Figure S1. Sample of posterior draws for the distance−based decay of covariance of abundance and trend among BBS routes for Baird's Sparrow (Centronyx bairdii) estimated using an isotropic spatial Gaussian Process model. The modeled estimates show that the covariance among routes in relative abundance of the species decreases very quickly with increasing distance (green lines), while the covariance among routes in trends decreases very slowly with distance (blue lines).

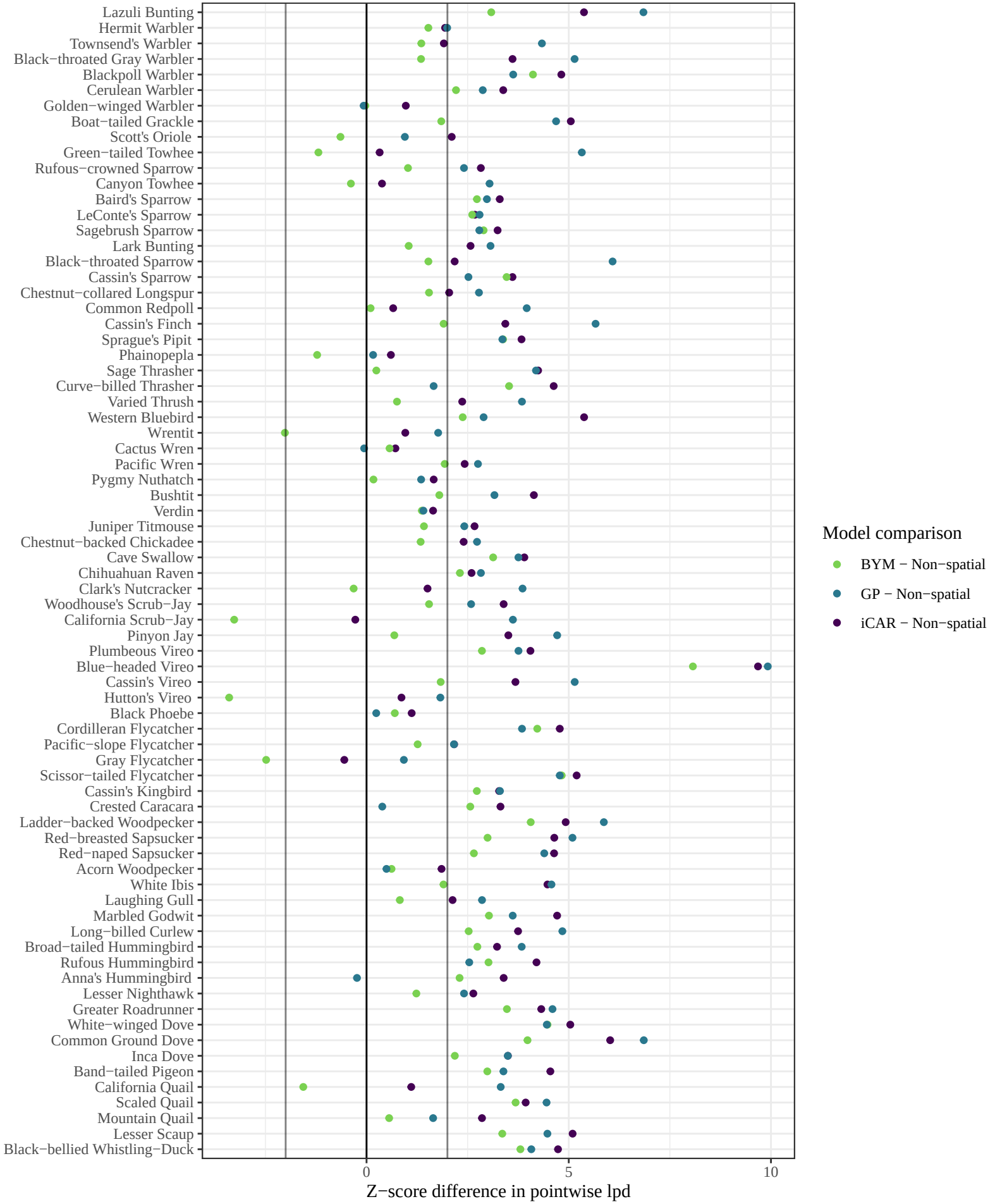

Figure S4. Leave Future Out (LFO) cross−validation results for 71 small−range species from the BBS database, comparing three explicitly spatial models (iCAR, BYM, and GP) to an otherwise identical non−spatial model. The values represent z−score summaries of the difference between each of the spatial models and the non−spatial model. For all of the comparisons, positive values indicate that the spatial model had higher out−of−sample predictive accuracy (higher log point−wise predictive density, lppd) than the non−spatial model.

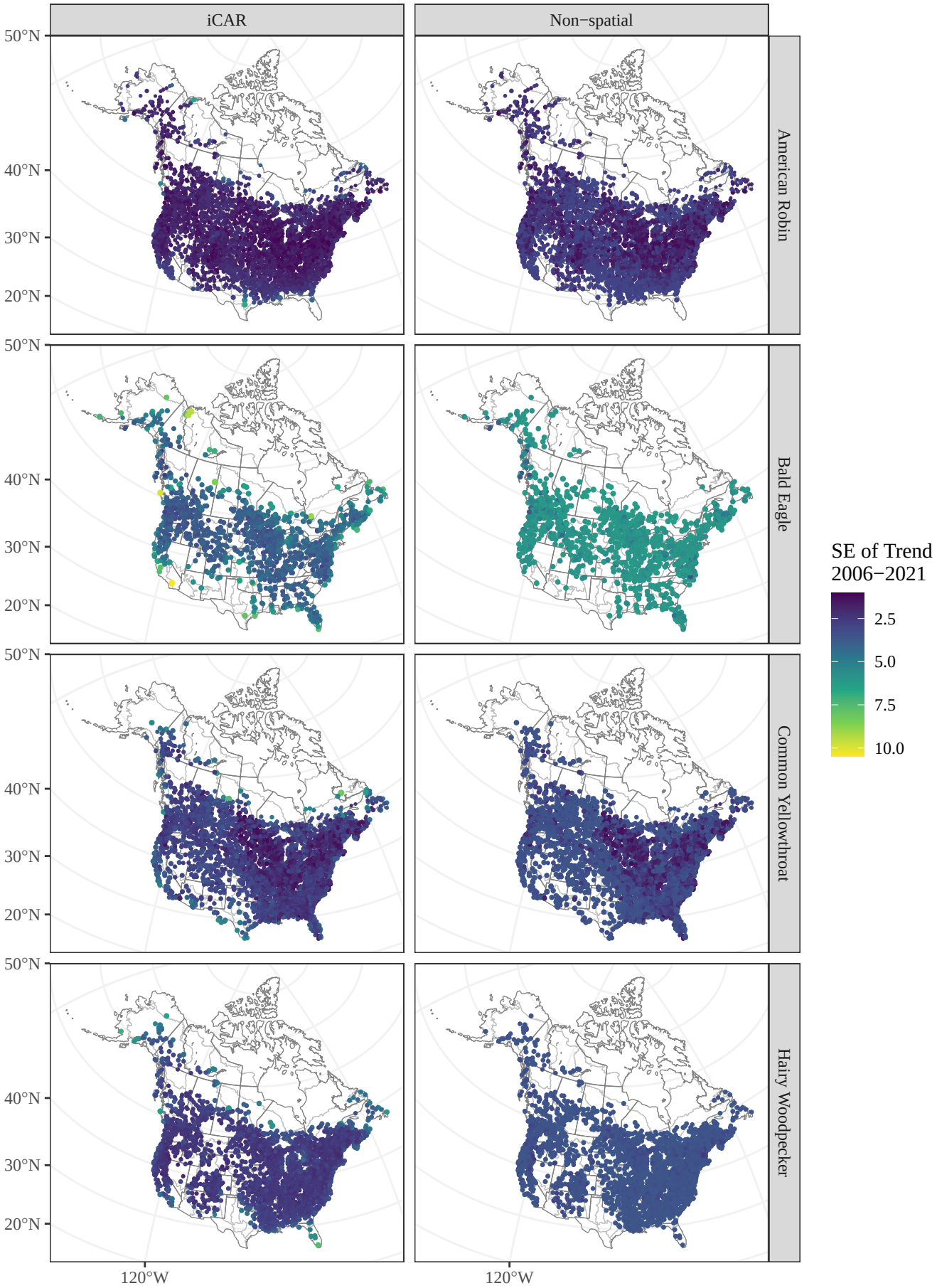

Figure S5. Examples of the spatial patterns in standard error of route−level trend estimates for four broad−ranging species from an iCAR spatial model and an otherwise identical non−spatial model. Each point represents the starting location of a Breeding Bird Survey route.

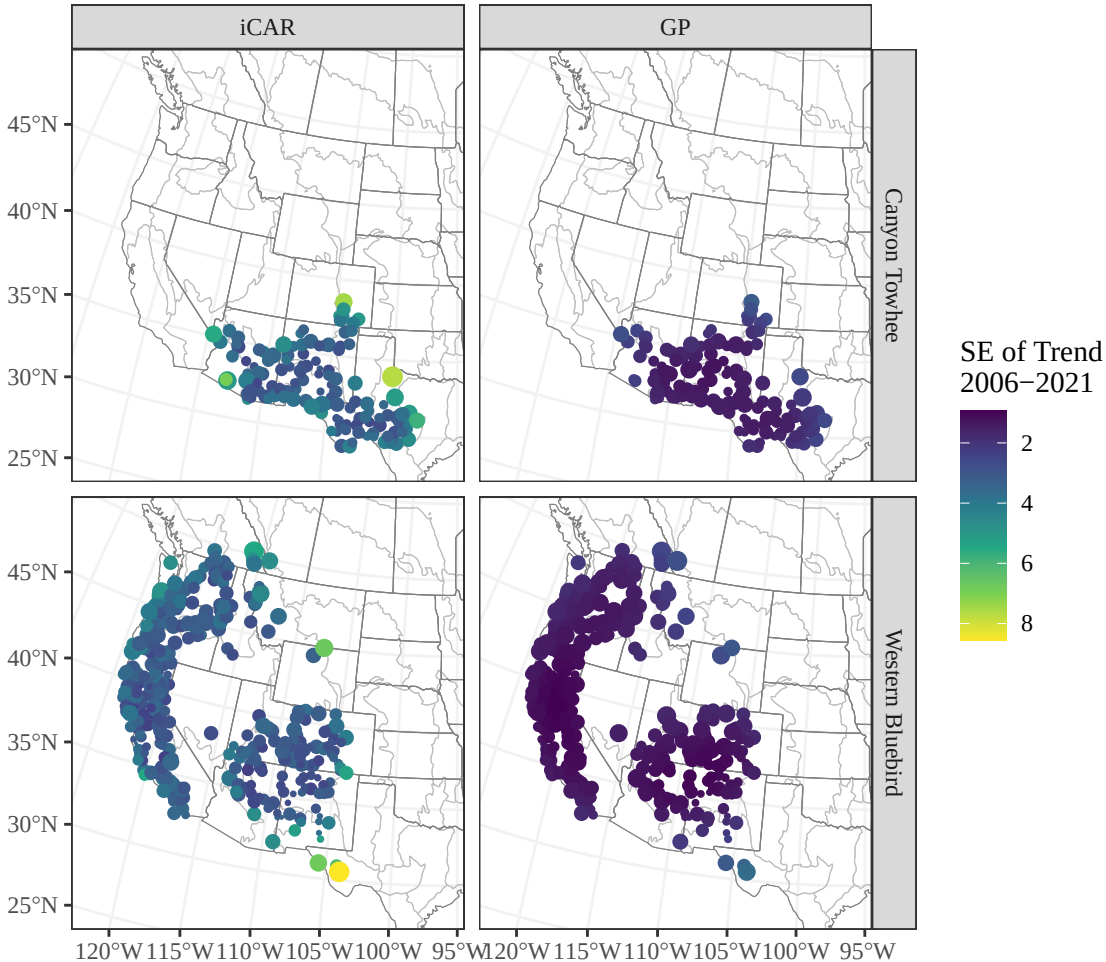

Figure S6. Map of standard error of route−level trend estimates for two species from two spatial models. Although the standard errors of the GP model's estimates are smaller than those of the iCAR model for both species, this higher estimated precision does not reflect higher accuracy because the out−of−sample predictive accuracy suggests that the best model varies between these two species. For Canyon Towhee (Melozone fusca) the GP model has higher accuracy and for Western Bluebird (Sialia mexicana) the iCAR model has higher accuracy.

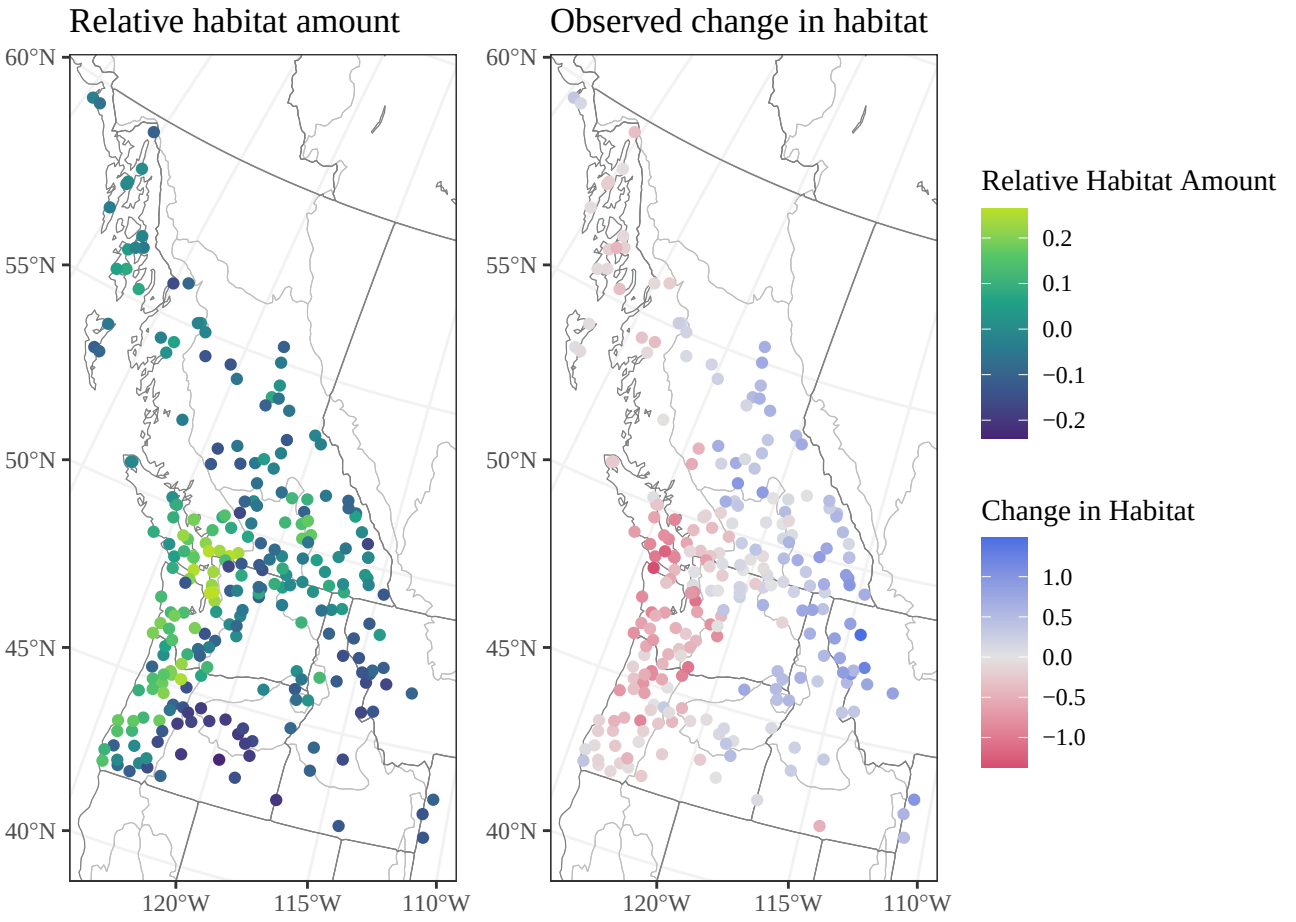

Figure S7. Map of route−level habitat covariates for Rufous Hummingbird from 2006−2021. The left plot shows the relative distribution of mean annual habitat amount. The right plot shows the distribution of the changes in habitat between 2006−2021. These maps demonstrate the general east−west pattern in both habitat amount and habitat change, where habitat has decreased in western portion of the species' range and increased in the east.

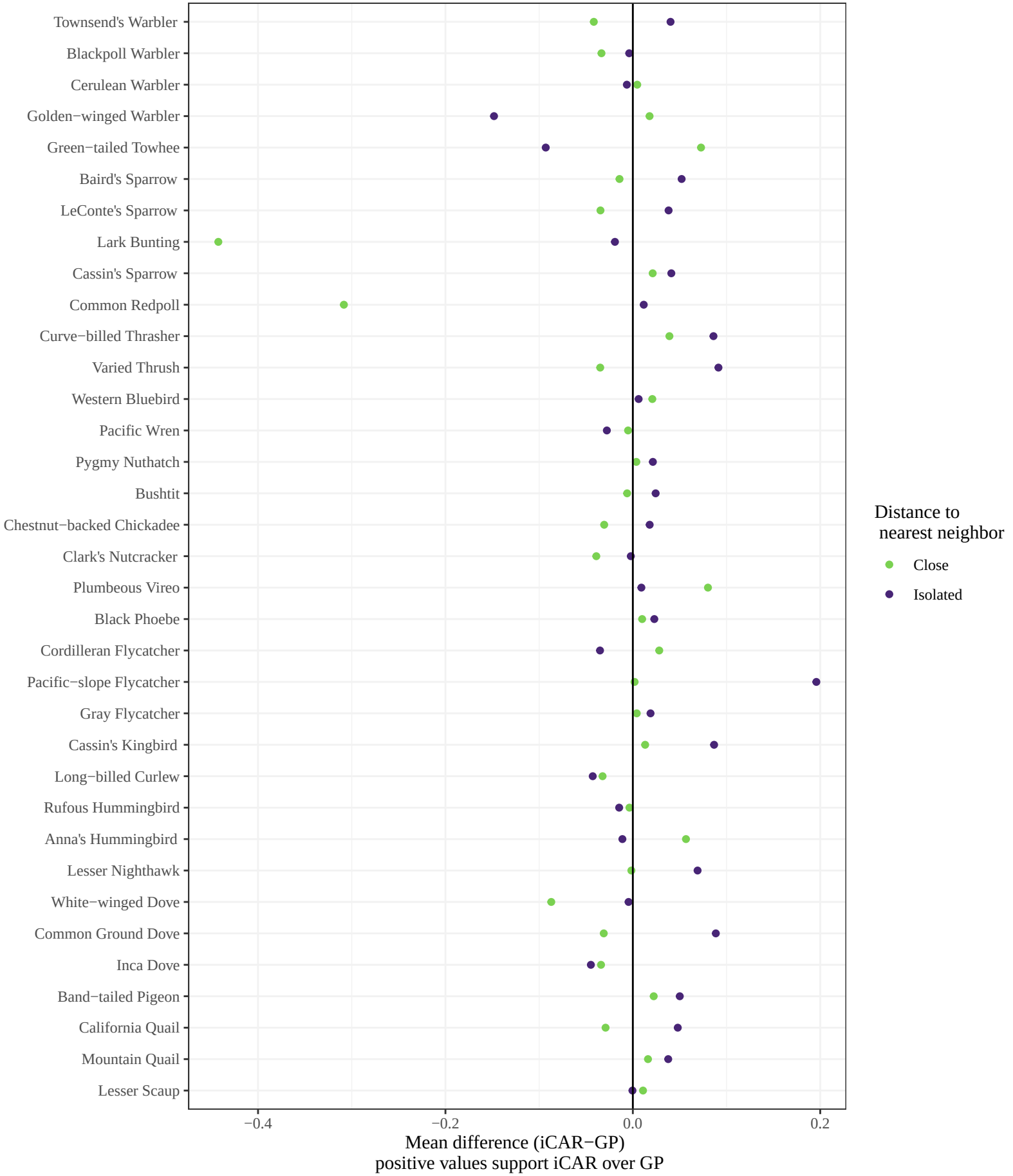

Figure S8. Mean point−wise differences in log posterior predictive density (lppd, iCAR−GP) between iCAR and GP spatial models for BBS routes that are Isolated from other routes (i.e., greater than 200 km from the nearest neighbour, in dark purple) and other routes that are more central to the species range and therefor have closer (and usually more) neighbors. For most of the species here, the iCAR based simplification of spatial relationships has higher predictive accuracy for the trends on Isolated routes than the GP model (dark points to the right of the vertal line at 0) that uses precise distance information and therefore necessarily treats these isolated routes as having lower covariance in trends and abundances than the iCAR model that treats them as immediate neighbours of the nearest routes that are 200 km away.

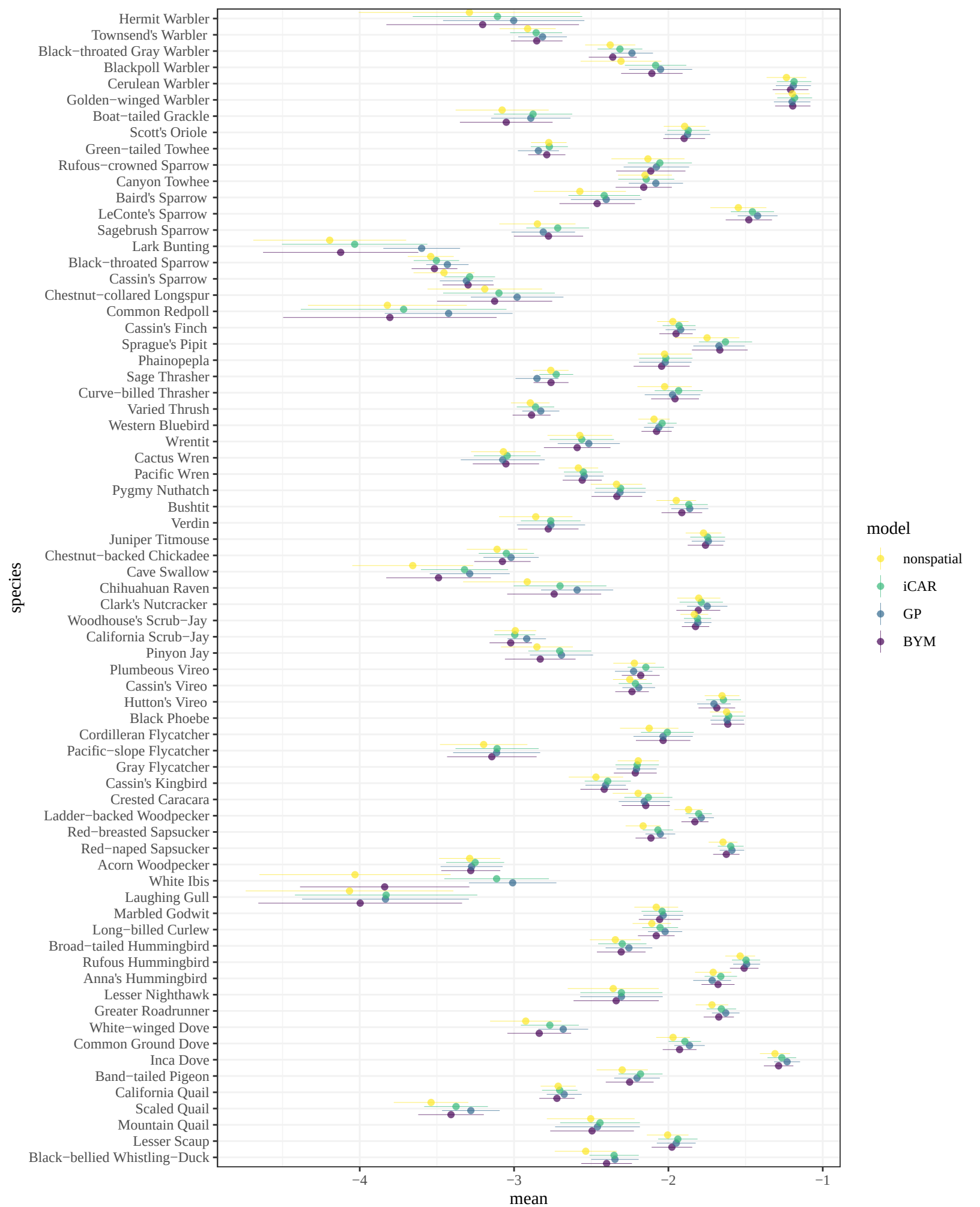

Figure S9. Mean point−wise log posterior predictive density (lppd) by species and model for three spatial models (iCAR, GP, and BYM) and one non−spatial model estimating trends and abundance at individual BBS routes.